J. Fluid Mech. (1989), *vol.* 201, *pp.* 323–356
Printed in Great Britain

Lubricated pipelining: stability of core–annular flow

By LUIGI PREZIOSI, KANGPING CHEN AND DANIEL D. JOSEPH

Department of Aerospace Engineering and Mechanics, University of Minnesota, Minneapolis, MN 55455, USA

(Received 5 October 1987 and in revised form 28 September 1988)

The stability of core–annular flow (CAF) in pipes is analysed using the linear theory of stability. Attention is confined to the potentially stable case of lubricated pipelining with the less viscous liquid, say water, in the annulus. The effects of surface tension and density are included, but gravity is excluded. We find upper and lower branches of the neutral curve in a Reynolds number ($\mathbb{R}$) *vs.* wavenumber (α) plane. A window of parameters is identified in which CAF is stable to small disturbances. When $\mathbb{R}$ is below the lower critical value, CAF is destabilized by surface tension and long waves break up into slugs and bubbles. The sizes of slugs and bubbles of oil in water observed by Charles, Govier & Hodgson (1961) are given by the wavelength of the fastest growing long wave. This long-wave instability is a capillary instability, modified by shear, which reduces to Rayleigh's instability in the appropriate limit. At higher $\mathbb{R}$, the capillary instability is stabilized by shear. At yet higher $\mathbb{R}$, above the upper critical value, the flow is unstable to generally shorter waves which leads to emulsification, water droplets in oil. The theory agrees with experiments. The analysis seems to be applicable to the design of lubricated pipelines; for example, there is an optimum viscosity ratio for stability, greater stability can be obtained by using heavy liquid as a lubricant when the flow is unstable to capillary modes on the lower branch and by using light liquids when the flow is unstable to emulsifying disturbances on the upper branch.

1. Introduction

There is a strong tendency for two fluids to arrange themselves so that the low-viscosity constituent is in the region of high shear (Joseph, Nguyen & Beavers 1984). This gives rise to a kind of gift of nature in which the lubricated flows are stable, and it opens up very interesting possibilities for technological applications in which one fluid is used to lubricate another.

We can imagine that it may be possible to introduce a beneficial effect in any flow of very viscous liquid important in applications by introducing small amounts of lubricating fluid. Nature's gift is evidently such that the lubricating fluid will migrate to the right places so as to do the desired job.

There are significant reserves of heavy viscous crude oils in the United States, Canada, Venzuela and Europe. Heavy crudes may have viscosities of 1000 P at room temperature. These viscous crudes cannot be transported by the usual pipeline methods. It is customary to reduce the viscosity of the oil either through the addition of a hydrocarbon diluent or through the installation of heating equipment at short intervals along the pipeline. The former method can only be used in the unusual case

in which there is an abundant supply of light oil in the same region as the heavy oil; heating is inconvenient and costly.

Another method which has been proposed to facilitate the transport of viscous crudes is the addition of an immiscible lubricating liquid, usually water. Experiments to examine this possibility have been carried out by Russell & Charles (1959), Russell, Hodgson & Govier (1959), Charles, Govier & Hodgson (1961), Gemmell & Epstein (1962) and Charles & Lilleleht (1966). Oliemans & Ooms (1986) have written a comprehensive review of pipe flows of oil and water, theory and experiment, prior to 1984.

Various arrangements of the oil and water occur in the aforementioned experiments. This type of non-uniqueness is typical of flowing bicomponent fluids. The arrangements that appear in horizontal pipes are: (*a*) stratified flow with heavy fluid below; (*b*) concentric oil in water (core–annular) flow; (*c*) water drops in oil; (*d*) oil drops (bubbles) in water (these include large bubbles and slugs of oil lubricated by water).

The measured pressure drops indicated that the addition of water can greatly reduce the pressure gradient. There is a powerful tendency for the water to migrate to the pipe walls where the shearing is greatest, lubricating the flow.

It was found that the core–annular flow had the greatest volume flux for a given pressure drop among all of the realized rearrangements. The pressure drop over the pipe could be even smaller than the pressure drop in water alone at the same value of the volume flux. The lubricating water layer was 10–40% of the pipe diameter. The power requirements for moving the small amount of water in core–annular flow is negligible.

Under widely applicable conditions, thin films of all kinds of lubricating layers are stable. Theoretical results, using standard methods of linearized stability theory, are listed below. Yih (1967) studied the stability of plane Couette flow in two layers separated by a planar interface with respect to long waves. He suppressed the effects of gravity and density differences and focused his attention on the viscosity difference and the volume ratio. He found that some of the these flows are stable and others unstable. Flows with a small layer of less viscous fluid on one wall, which we call lubricating flows, are stable. Hooper & Boyd (1983) considered the stability of Couette flow of two fluids separated by a plane layer in an infinite region, without boundaries. They find that the flow with a flat free surface is always unstable to very short waves when the surface tension is neglected. Surface tension stabilizes the shortest waves. Renardy (1985) and Hooper & Boyd (1987) studied the stability of layered Couette flow to disturbances of arbitrary wavelength. They show that the only stable flow with a flat interface at small Reynolds numbers, tending to zero, has a finite surface tension and is a lubricating flow.

Hickox (1971) studied the stability of Poiseuille flow of two fluids when the less viscous fluid is centrally located. He showed that all such flows are unstable. Joseph, Renardy & Renardy 1983, 1984 (hereinafter JRR 1983 and JRR 1984 respectively) studied the stability of Poiseuille flow of two fluids when the more viscous fluid is centrally located. They found this flow, with an interface of constant radius, is stable provided that the layer of less viscous fluid on the wall of the pipe is small. Than, Rosso & Joseph (1987) studied the analogous problem for plane Poiseuille flow, restricting perturbations to long waves. They found that the flows with thin fluid inside were unstable and that the lubricating flows with thick fluid inside were always stable, independent of the volume ratio. Y. Renardy & Joseph (1985) studied the stability of rotating Couette flow in two circular layers. Again, the only stable

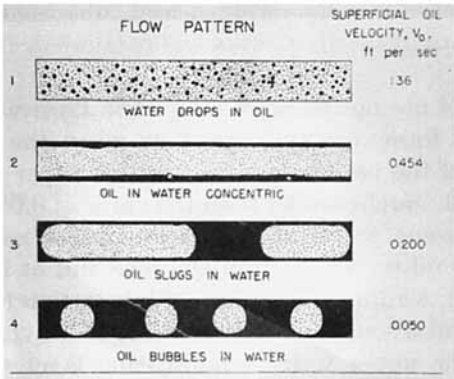

Figure 3 — Drawings prepared from photographs of the 16.8 viscosity oil flowing in the presence of water and showing the variation in flow pattern with oil velocity for a low fixed water velocity of 0.10 ft./sec.

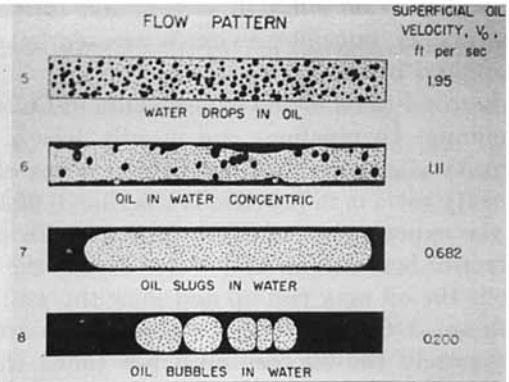

Figure 4 — Drawings prepared from photographs of the 16.8 centipoise viscosity oil flowing in the presence of water and showing the variation in flow pattern with oil velocity for a fixed water velocity of 0.682 ft./sec.

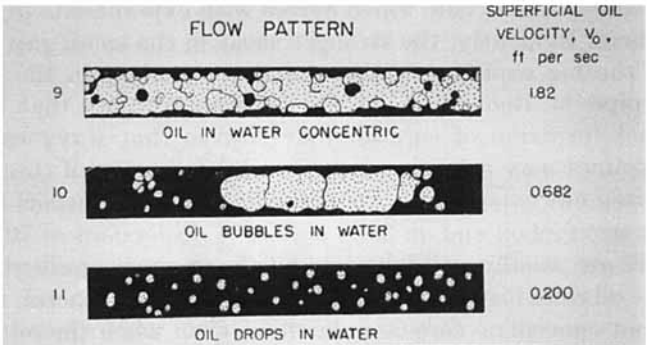

Figure 5 — Drawings prepared from photographs of the 16.8 centipoise viscosity oil flowing in the presence of water and showing the variation in flow pattern with oil velocity for a high fixed water velocity of 2.04 ft./sec.

FIGURE 1. The sketches reproduced above are taken from the paper by Charles, Govier & Hodgson (1961). The experiments are discussed and the results compared with theory in §13.

flows with a cylindrically perfect interface are the lubricating flows, with a thin layer of less viscous liquid on one of the cylinders. The stabilizing effect of lubrication can be strong enough to overcome centrifuging when the lubricating fluid on the inner cylinder is heavy.

In this paper, we study the stability of core–annular flow with viscous fluid in the core using the linear theory of stability. Our analysis goes beyond that given by JRR, because the effects of surface tension and density differences, neglecting gravity, are considered. Surface tension is very important. It is not possible to derive a theory without it that could be used in the design and control of lubricated-pipeline technologies.

The results computed here, taken together with that given in JRR, appear to be in quantitative agreement with the results of experiments of Charles, Govier & Hodgson (1961, hereinafter referred to as CGH) on bicomponent flow of water and oil–carbon tetrachloride solutions density matched with water. Gravity is made negligible by density matching, so that their experiments and our analysis are compatible. Their results are summarized in figure 1 and discussed in §13. For now, it will suffice to note that (*a*) there is a minimum speed, observed in experiments, but not previously treated by analysis, below which core–annular flow is unstable and

gives way to oil slugs in water; and (*b*) there is a maximum speed, observed in experiments, but not previously treated by analysis, above which core–annular flow is replaced by emulsions of water in oil.

The conditions of the experiments of CGH are not those of interest in lubricated pipelining. In pipelines one usually sees a form of wavy core flow when the oil viscosity is greater than 500 CP. In terms of the parameters used in this paper the viscosity ratio m in practice is less than 0.002, much smaller than the value of 0.0532 for the experiments of CGH. Moreover, in some practical applications the density difference between oil and water causes the oil to ride high in the pipe and at low speeds the oil may rise up and seize the wall, leading to a failure of lubrication (see Oliemans & Ooms 1986 for a photograph and discussions of the effects of gravity). Fortunately the oil core need not touch the upper wall. A lubricating layer can persist. The exact hydrodynamics, which maintain the lubrication layer at the top of the pipe, is not understood. Oliemans & Ooms think that a lubrication effect associated with ripples is important. Oliemans (1986) has developed a lubricating-film model for core–annular flow which agrees with experiments in some details and disagrees in others. Evidently, the stronger shear in the small gap at the top of the pipe stabilizes the big capillary waves which are evident in the large gap at the bottom of the pipe. M. Renardy & Joseph 1986 have shown that travelling ripples will occur as a bifurcation of core annular flow so that wavy core flow which is observed in pipelines may arise as a subcritical bifurcation of core–annular flow.

We have carried out experiments on water-lubricated transport of SAE 30 motor oil and number two fuel oil and on 30% and 40% dispersions of 70 μm coal in these two oils. The oils are usually well lubricated if the pressure gradient is not too small, even though the oil rides high in the pipe due to gravity. In general, we get lubricated flows, though not concentric core–annular flow, even when the oil at the top seizes the wall. In these cases the oil in the core is still lubricated by a film of water which lies underneath the oil on the top of the pipe and the oil core below it. The effects of gravity are not so serious as to impede successful lubrication in our small pipes, but these effects could be more serious in pipes of larger diameter. There are some interesting situations in which the density of the oil and water are nearly the same, so that the gravity effects are greatly diminished. This is the case, for example, with heavy oil extracted from the Alberta oil sands and with the dispersions of 40% coal in SAE 30 motor used in our experiments. The most serious problem for the technology of water–lubricated pipelining associated with stratification due to gravity is start-up from rest. The effects of gravity under transient and steady conditions have not yet been treated in a theoretically satisfactory manner.

In this paper we confine our attention to parameter values in the range of the experiments of CGH. The second type of failure of lubricated pipelining, emulsification of water in oil, already occurs in these experiments and is apparently correlated with the higher-Reynolds-number instability identified in our linear theory. In a second paper (Part 2 of this paper, by H. Hu & D. D. Joseph), we implemented a finite-element program with an adaptive mesh in the boundary layer at the wall. The finite-element calculation agrees perfectly with the pseudospectral code used in the present calculation but it also works well at the small values of $m < 0.002$ characteristic of field practice. We compared the results of our finite-element calculation with field data provided from experiments in 6 in. diameter pipes. The linear theory predicted wavy core flow when the oil viscosity was greater than a critical one, with emulsification of water into oil for smaller viscosities. These predictions agree with the field data.

2. The equations and basic flow

Two liquids are flowing down a pipe of inner radius R_2. The interface between the two liquids is given by $r = R(\theta, x, t)$ where (r, θ, x) are cylindrical coordinates and $\hat{\boldsymbol{U}} = (\hat{U}, \hat{V}, \hat{W})$ are the corresponding components of velocity. The region $0 \leqslant r \leqslant R(\theta, x, t)$ is occupied by the first liquid with viscosity and density μ_1 and ρ_1 and the second liquid (μ_2 and ρ_2) is located in $R(\theta, x, t) \leqslant r \leqslant R_2$. The pipe axis is at $r = 0$ and the pipe is infinitely long $-\infty \leqslant x \leqslant \infty$. The mean value of R over $\theta, 0 \leqslant \theta \leqslant 2\pi$ is $R_1 = \bar{R}(\theta, x, t)$, a constant fixed by the prescribed volumes of each of the two liquids, independent of t.

The equations of motion, gravity neglected, are

$$\rho_l \frac{\mathrm{d}\hat{\boldsymbol{U}}}{\mathrm{d}t} = -\nabla\hat{P} + \mu_l \nabla^2 \hat{\boldsymbol{U}}, \quad \operatorname{div} \hat{\boldsymbol{U}} = 0, \tag{2.1}$$

where $l = 1$ when $0 \leqslant r \leqslant R$ and $l = 2$ when $R \leqslant r \leqslant R_2$,

$$\hat{\boldsymbol{U}} = \boldsymbol{0} \quad \text{on} \quad r = R_2, \tag{2.2}$$

and $\hat{\boldsymbol{U}}$ is bounded at $r = 0$. The equations on the interface are

$$\hat{U} = \frac{\partial R}{\partial t} + \hat{W}\frac{\partial R}{\partial x} + \frac{\hat{V}}{R}\frac{\partial R}{\partial \theta}, \quad \bar{R} = R_1, \tag{2.3}$$

$$[\![\hat{U}]\!] \overset{\text{def}}{=} (\hat{U})_1 - (\hat{U})_2 = 0 \tag{2.4}$$

is the jump in $\hat{U}$ over $r = R$, and

$$-([\![\hat{P}]\!] + 2HT)\boldsymbol{n} + [\![2\mu \boldsymbol{D}[\hat{\boldsymbol{U}}]]\!] \cdot \boldsymbol{n} = 0, \tag{2.5}$$

where $\boldsymbol{D}[\hat{\boldsymbol{U}}] = \frac{1}{2}(\nabla\hat{\boldsymbol{U}} + \nabla\hat{\boldsymbol{U}}^{\mathrm{T}})$, $2H$ is the sum of the principal curvatures, T is the coefficient of surface tension, $\boldsymbol{n} = \boldsymbol{n}_{12}$ is the normal to $r - R = 0$ from liquid 1 to 2.

We shall study the stability of core–annular flow

$$\left.\begin{aligned} \hat{\boldsymbol{U}} &= (0, 0, W(r)), \\ [\![\hat{P}]\!] &= [\![P]\!] = T/R_1 \end{aligned}\right\} \tag{2.6}$$

where $\nabla P = -\boldsymbol{F}, F > 0$ is the magnitude of the constant pressure gradient, and

$$W(r) = \left\{\begin{aligned} &-\frac{F}{4\mu_1}(r^2 - R_1^2) + \frac{F}{4\mu_2}(R_2^2 - R_1^2), && 0 \leqslant r \leqslant R_1, \\ &\frac{F}{4\mu_2}(R_2^2 - r^2), && R_1 \leqslant r \leqslant R_2. \end{aligned}\right\} \tag{2.7}$$

To study the stability and bifurcation of core–annular flow, it is necessary to introduce an extended core–annular flow, where in (2.7) we write $0 \leqslant r \leqslant R(\theta, x, t)$ and $R(\theta, x, t) \leqslant r \leqslant R_2$, respectively.

3. Perturbation equations

We now perturb extended core–annular flow

$$\hat{U} = (u, v, W+w), \quad \hat{P} = P+p, \quad R = R_1+\delta(\theta, x, t) \tag{3.1}$$

and consider the linearized equations for (u, v, w, p, δ).

$$\left.\begin{aligned} \rho_l\left[\frac{\partial u}{\partial t}+W\frac{\partial u}{\partial x}\right] &= -\frac{\partial p}{\partial r}+\mu_l\left[\nabla^2 u-\frac{u}{r^2}-\frac{2}{r^2}\frac{\partial v}{\partial \theta}\right], \\ \rho_l\left[\frac{\partial v}{\partial t}+W\frac{\partial v}{\partial x}\right] &= -\frac{1}{r}\frac{\partial p}{\partial \theta}+\mu_l\left[\nabla^2 v-\frac{v}{r^2}+\frac{2}{r^2}\frac{\partial u}{\partial \theta}\right], \\ \rho_l\left[\frac{\partial w}{\partial t}+W\frac{\partial w}{\partial x}+W'u\right] &= -\frac{\partial p}{\partial x}+\mu_l\nabla^2 w, \quad \frac{1}{r}\frac{\partial}{\partial r}(ru)+\frac{1}{r}\frac{\partial v}{\partial \theta}+\frac{\partial w}{\partial x} = 0, \end{aligned}\right\} \tag{3.2}$$

where $(\rho_l, \mu_l) = (\rho_1, \mu_1)$ in $r < R_1$ and (ρ_2, μ_2) in $r > R_1$ and $W' = \mathrm{d}W/\mathrm{d}r$. Moreover,

$$u = v = w = 0 \quad \text{at} \quad r = R_2, \tag{3.3}$$

u, v, w are bounded at $r = 0$ and satisfy other conditions to be stated later. On the interface at $r = R_1$, we find that

$$u = W\delta_x+\delta_t, \quad \bar{\delta} = 0, \tag{3.4a}$$

$$[\![u]\!] = [\![v]\!] = 0, \tag{3.4b}$$

$$\left[\!\!\left[\mu\left(\frac{\partial u}{\partial x}+\frac{\partial w}{\partial r}\right)\right]\!\!\right] = 0, \tag{3.4c}$$

$$\left[\!\!\left[\mu\left(\frac{\partial u}{\partial \theta}+R_1\frac{\partial v}{\partial r}-v\right)\right]\!\!\right] = 0, \tag{3.4d}$$

$$-[\![p]\!]+2\left[\!\!\left[\mu\frac{\partial u}{\partial r}\right]\!\!\right] = \frac{T}{R_1^2}(\delta_{\theta\theta}+R_1^2\delta_{xx}+\delta) \tag{3.4e}$$

and

$$[\![W']\!]\,\delta+[\![w]\!] = 0. \tag{3.5}$$

Equation (3.5) shows that w is not continuous across $r = R_1$, and it can produce instability. We can eliminate $\delta = -[\![w]\!]/[\![W']\!]$ from our problem.

4. Dimensionless equations and parameters

We shall now make our equations dimensionless. Lengths are scaled with the mean radius R_1, velocity is scaled with the centreline velocity

$$W_0 = F\{R_1^2(\mu_2-\mu_1)+R_2^2\mu_1\}/4\mu_1\mu_2$$

and time with R_1/W_0. After introducing these scales, we find equations in dimensionless variables. We shall use the same symbols for dimensional and dimensionless variables.

The differential equations satisfied by the dimensionless u, v, w, p are of the same form as (3.2) with $\rho_l = 1$ and μ_l replaced by $1/\mathbb{R}_l$ where

$$\mathbb{R}_l = \rho_l W_0 R_1/\mu_l, \quad l = 1, 2. \tag{4.1}$$

A dimensionless function $W(r)$ also appears in these equations and is given by

$$W(r) = \begin{cases} 1-mr^2/(a^2+m-1), & 0 \leqslant r \leqslant 1 \\ (a^2-r^2)/(a^2+m-1), & 1 \leqslant r \leqslant a, \end{cases} \tag{4.2}$$

where $$m = \mu_2/\mu_1 \leqslant 1$$

is the viscosity ratio, and $$a = R_2/R_1 \geqslant 1$$

is the dimensionless radius of the outer cylinder. The ratio of the volume of the liquid outside to the volume of liquid is a^2-1. The boundary conditions (3.3) are required to hold at $r = a$. Equation (4.2) shows that $W(r)$ is continuous across $r = 1$,

$$W(1) = (a^2-1)/(a^2+m-1), \tag{4.3}$$

but, because the shear stress is continuous, the derivatives of W are different on sides 1 and 2 of $r = 1$

$$\left.\begin{aligned} W_1'(1) &= -2m/(a^2+m-1), \\ W_2'(1) &= -2/(a^2+m-1). \end{aligned}\right\} \tag{4.4}$$

The dimensionless interface is at $r = 1$. Equations (3.4*a*, *b*) and (3.5) are unchanged in form. Equations (3.4*c–e*) take the following form in dimensionless variables:

$$\left[\!\left[\frac{\zeta}{\mathbb{R}}\left(\frac{\partial u}{\partial x}+\frac{\partial w}{\partial r}\right)\right]\!\right] = 0, \tag{4.5}$$

$$\left[\!\left[\frac{\zeta}{\mathbb{R}}\left(\frac{\partial u}{\partial \theta}+\frac{\partial v}{\partial r}-v\right)\right]\!\right] = 0, \tag{4.6}$$

$$-[\![\zeta p]\!] + 2\left[\!\left[\frac{\zeta}{\mathbb{R}}\frac{\partial u}{\partial r}\right]\!\right] = S(\delta_{\theta\theta}+\delta_{xx}+\delta), \tag{4.7}$$

where p_i is scaled by $\rho_i W_0^2$, $$\zeta_i = \frac{\rho_i}{\rho_\iota}, \tag{4.8}$$

is a density ratio and $$S = \frac{T}{\rho_1 W_0^2 R_1} \tag{4.9}$$

is the dimensionless surface tension.

The parameter S has been used in all previous studies of instability of two fluids, but it is not a good parameter because it depends strongly on the velocity or the rate of shear in the basic flow. It is better to write

$$S = \frac{J}{\mathbb{R}_1^2}, \quad J = \frac{TR_1}{a\rho_1 \nu_1^2} \tag{4.10}$$

where J is a surface-tension parameter introduced by Chandrasekhar (1961) in his study of capillary instability of jets of viscous liquid in air.

For core–annular flow the parameter $J^* = TR_2/\rho_1 \nu_1^2$ is more convenient than J because

$$J^* = aJ \tag{4.11}$$

is given when the oil and pipe radius are known.

The problem is characterized by six dimensionless parameters: m, a, ζ_2, J, $\mathbb{R}_1$ and $\mathbb{R}_2$ of which five are independent, $\mathbb{R}_1/\mathbb{R}_2 = m/\zeta_2$, where $m = \mu_2/\mu_1$.

5. Normal modes

We replace $[u_l, v_l, w_l, p_l](r,\theta,x,t)$ and $\delta(\theta,x,t)$ with amplitude functions $[iu_l, v_l, w_l, p_l](r)$ and an amplitude constant δ times $\exp[in\theta + i\alpha(x-Ct)]$ in the usual way. The equation

$$u(1,\theta,x,t) = \delta_t + W(1)\,\delta_x$$

then reduces to

$$u(1) = \alpha(W(1)-C)\,\delta, \tag{5.1}$$

giving δ. In each of the two regions, corresponding to $l = 1 (0 \leqslant r \leqslant 1)$ and $l = 2 (1 \leqslant r \leqslant a)$, we get

$$u' + \frac{u}{r} + \frac{n}{r}v + \alpha W = 0, \tag{5.2}$$

$$\alpha(W_l - C)\,u = p' - \frac{\mathrm{i}}{\mathbb{R}_l}\left\{u'' + \frac{u'}{r} - \left(\alpha^2 + \frac{n^2+1}{r^2}\right)u - \frac{2n}{r^2}v\right\}, \tag{5.3}$$

$$\alpha(W_l - C)\,v = -\frac{np}{r} - \frac{\mathrm{i}}{\mathbb{R}_l}\left\{v'' + \frac{v'}{r} - \left(\alpha^2 + \frac{n^2+1}{r^2}\right)v - \frac{2n}{r^2}u\right\}, \tag{5.4}$$

$$\alpha(W_l - C)\,w + W_l' u = -\alpha p - \frac{\mathrm{i}}{\mathbb{R}_l}\left\{w'' + \frac{w'}{r} - \left(\alpha^2 + \frac{n^2}{r^2}\right)w\right\}. \tag{5.5}$$

The boundary values of the amplitude functions are such that

$$u(a) = v(a) = w(a) = 0, \qquad u(0), v(0), w(0), p(0) \text{ finite}. \tag{5.6}$$

On the interface $r = 1$, we have

$$[\![u]\!] = [\![v]\!] = 0, \tag{5.7}$$

$$[\![W']\!]\,u(1) + \alpha(W(1)-C)\,[\![w]\!] = 0, \tag{5.8}$$

$$\left[\!\left[\frac{\zeta}{\mathbb{R}}(w' - \alpha u)\right]\!\right] = 0, \tag{5.9}$$

$$\left[\!\left[\frac{\zeta}{\mathbb{R}}(v' - v - nu)\right]\!\right] = 0, \tag{5.10}$$

$$-[\![\zeta p]\!] + 2\mathrm{i}\left[\!\left[\frac{\zeta}{\mathbb{R}}u'\right]\!\right] = \frac{J}{\mathbb{R}_1^2}(1-\alpha^2-n^2)\frac{u(1)}{\alpha(W(1)-C)}. \tag{5.11}$$

We eliminated p from the system (5.2)–(5.11). Equations (5.3) and (5.4) are reduced to

$$\frac{\mathrm{i}}{\mathbb{R}_l}u'' + \left(\frac{\mathrm{i}}{\mathbb{R}_l}\frac{1}{r} + \frac{W_l'}{\alpha}\right)u' - \left\{\frac{\mathrm{i}}{\mathbb{R}_l}\left(\alpha^2 + \frac{n^2+1}{r^2}\right) - \frac{W_l''}{\alpha} - \alpha(W_l - C)\right\}u - \frac{2\mathrm{i}n}{\mathbb{R}_l}\frac{1}{r^2}v$$

$$+ \frac{\mathrm{i}}{\alpha\mathbb{R}_l}w''' + \frac{\mathrm{i}}{\alpha\mathbb{R}_l}\frac{1}{r}w'' - \left\{\frac{\mathrm{i}}{\alpha\mathbb{R}_l}\left(\alpha^2 + \frac{n^2+1}{r^2}\right) - (W_l - C)\right\}w' + \left\{\frac{2\mathrm{i}n^2}{\alpha\mathbb{R}_l}\frac{1}{r^3} + W_l'\right\}w = 0 \tag{5.12}$$

and

$$\left\{\frac{2\mathrm{i}}{\mathbb{R}_l}\frac{1}{r^2} + \frac{W_l'}{\alpha}\frac{1}{r}\right\}nu - \frac{\mathrm{i}}{\mathbb{R}_l}v'' - \frac{\mathrm{i}}{\mathbb{R}_l}\frac{1}{r}v' + \left\{\frac{\mathrm{i}}{\mathbb{R}_l}\left(\alpha^2 + \frac{n^2+1}{r^2}\right) - \alpha(W_l - C)\right\}v + \frac{n\mathrm{i}}{\alpha\mathbb{R}_l}\frac{1}{r}w''$$

$$+ \frac{n\mathrm{i}}{\alpha\mathbb{R}_l}\frac{1}{r^2}w' - \frac{n}{r}\left\{\frac{\mathrm{i}}{\alpha\mathbb{R}_l}\left(\alpha^2 + \frac{n^2}{r^2}\right) - (W_l - C)\right\}w = 0, \tag{5.13}$$

where $(\mathbb{R}_l, W_l)$ correspond to regions 1 and 2.

We eliminate $[\![\zeta p]\!]$ from the normal-stress condition (5.11) by equating to $[\![\zeta p]\!]$ obtained by evaluating (5.5) at $r = 1$. After some simplifications, using the other interface conditions, we get

$$\frac{J}{\mathbb{R}_1^2}(1-\alpha^2-n^2)\frac{[\![w]\!]}{[\![W']\!]}+2\mathrm{i}\left[\!\!\left[\frac{\zeta}{\mathbb{R}}u'\right]\!\!\right]+\frac{\mathrm{i}}{\alpha}\left[\!\!\left[\frac{\zeta}{\mathbb{R}}\{w''+w'-(\alpha^2+n^2)\,w\}\right]\!\!\right]$$
$$+(W-C)\left\{[\![w\zeta]\!]-\frac{[\![W'\zeta]\!]}{[\![W']\!]}[\![w]\!]\right\}=0. \quad (5.14)$$

The governing equations are (5.2), (5.6)–(5.10), (5.12), (5.13) and (5.14).

The conditions (5.6) at the origin may be stated more precisely using the method of Frobenius. Conditions may also be inferred from the fact that $\boldsymbol{u}(r,\theta,x,t)$ is single valued, hence independent of θ at $r = 0$ (see Joseph 1976, p. 23). We may decompose $\boldsymbol{u}$ into an axial part $\boldsymbol{e}_x w$ and a tangential part $\boldsymbol{e}_t u_t = \boldsymbol{e}_r u + \boldsymbol{e}_\theta v$. Of course, $w(0,x)\,\mathrm{e}^{\mathrm{i}n\theta}$ is independent of θ when $n = 0$, or when $n \neq 0$ and $w(0,x) = 0$. The tangential velocity

$$u_t = \cos\theta[\mathrm{i}u(0,x)\,\mathrm{e}^{\mathrm{i}n\theta}]-\sin\theta[v(0,x)\,\mathrm{e}^{\mathrm{i}n\theta}]$$

is independent of θ when

$$\frac{\partial u_t}{\partial\theta}=-\{(nu+v)\cos\theta+\mathrm{i}\sin\theta(u+nv)\}\,\mathrm{e}^{\mathrm{i}n\theta}=0.$$

When $n \neq 1$, u_t is zero; then, $u(0,x) = v(0,x) = 0$. When $n = 1$, it is enough to have $u(0)+v(0) = 0$. The tangential component u_t need not vanish when $n = 1$. Some further conditions at $r = 0$ can be deduced from (5.2) at $r = 0$, using the results just obtained,

$$\lim_{r\to 0}\left\{\alpha w+u'+\frac{u+nv}{r}\right\}=\alpha w(0)+2u'(0)+nv'(0)=0.$$

Summarizing our results,

$$\left.\begin{aligned} &n=0: \quad u(0)=v(0)=\alpha w(0)+2u'(0)=0,\\ &n=1: \quad u(0)+v(0)=w(0)=0,\\ &n\geqslant 2: \quad u(0)=v(0)=w(0)=0. \end{aligned}\right\} \quad (5.15)$$

We define system I for u, v and w to be (5.2), (5.7)–(5.10), (5.12), (5.13) and (5.14). We also worked with the system II of equations for u and v alone which can be derived from system I by using (5.2) to eliminate w. System II is defined by the condition

$$u(a) = v(a) = u'(a) = 0 \quad (5.16a, b, c)$$

and the following equations in the two regions $l = 1, 2$ inside and outside the interface at $r = 1$:

$$\begin{aligned} &f_l \overset{\text{def}}{=} \mathrm{i}\alpha\mathbb{R}_l(W_l(r)-C)\,r^2,\\ &r^4u''''+2r^3u'''-[f_l+2\alpha^2r^2+n^2+3]\,r^2u''-[f_l+2\alpha^2r^2-n^2-3]\,ru'+[f_l(\alpha^2r^2+1)\\ &\quad+\alpha^4r^4+(n^2+2)\,\alpha^2r^2+3n^2-3]\,u+nr^3v'''-2nr^2v''\\ &\quad-[f_l+\alpha^2r^2+n^2-3]\,nrv'+[f_l-\mathrm{i}\alpha\mathbb{R}_l\,W_l'\,r^3\\ &\quad+3(\alpha^2r^2+n^2-1)]\,nv=0, \end{aligned} \quad (5.17)$$

$$nr^3u'''+2nr^2n''-[f_l+\alpha^2r^2+n^2+1]\,nru'-[f_l-\mathrm{i}\alpha\mathbb{R}_l\,W_l'\,r^3+3\alpha^2r^2+n^2-1]\,nu$$
$$+(a^2r^2+n^2)\,r^2v''+(\alpha^2r^2-n^2)\,rv'-[f_l(\alpha^2r^2+n^2)+\alpha^4r^4$$
$$+(2n^2+1)\,\alpha^2r^2+n^2(n^2-1)]\,v=0. \tag{5.18}$$

At the interface $r=1$, we have

$$[\![u]\!]=[\![v]\!]=0, \tag{5.19a, b}$$

$$(m-1)\,W_2'(1)\,u_2-(W(1)-C)\,[\![u']\!]=0, \tag{5.20}$$

$$v_1'-mv_2'+(m-1)\,v+n(m-1)\,u=0, \tag{5.21}$$

$$u_1''+u_1'+(\alpha^2+n^2-1)\,(1-m)\,u-mu_2''-mu_2'=0, \tag{5.22}$$

$$u_1'''+2u_1''-(f_1+3\alpha^2+n^2+1)\,u_1'+nv_1''-nv_1'$$
$$-mu_2'''-2mu_2''+[f_1\zeta_2+m(3\alpha^2+n^2+1)]\,u_2'$$
$$+[f_1(\zeta_2-1)-\mathrm{i}\alpha\mathbb{R}_1\,W_2'(1)\,(\zeta_2-m)+(m-1)\,(\alpha^2+n^2-1)]\,u$$
$$-nmv_2''+nmv_2'+[f_1(\zeta_2-1)+(m-1)\,(\alpha^2+n^2-1)]\,nv$$
$$+\frac{\mathrm{i}\alpha J}{\mathbb{R}_1(W(1)-C)}(\alpha^2+n^2-1)\,u=0. \tag{5.23}$$

Equation (5.23) may be put into a more convenient form, using (5.20),

$$u_1'''+2u_1''-(3\alpha^2+n^2+1)\,u_1'+nv_1''-nv_1'-mu_2'''-2mu_2''+\{f_1(\zeta_2-1)+m(3\alpha^2$$
$$+n^2+1)\}\,u_2'+\{f_1(\zeta_2-1)-\mathrm{i}\alpha\mathbb{R}_1(\zeta_2-1)\,W_2'(1)+(m-1)\,(\alpha^2$$
$$+n^2-1)\}\,u_2+\{f_1(\zeta_2-1)+(m-1)\,(\alpha^2+n^2-1)\}\,nv_2-nmv_2''$$
$$+nmv_2'+\frac{\mathrm{i}\alpha J(\alpha^2-n^2-1)}{\mathbb{R}_1(W(1)-C)}u_2=0. \tag{5.24}$$

In the axisymmetric case, when $n=0$, the equations for u and v decouple and the unstable eigenvalues are determined from the equations for $u(r)$. The v-equation gives rise only to stable eigenvalues. Most of the results given in this paper are computed for the case of matched density $\zeta_2=1$ and axisymmetric disturbances, $n=0$. In this case, u is governed by

$$r^4u''''+2r^3u'''-[f_l+2\alpha^2r^2+3]\,r^2u''-[f_l+2\alpha^2r^2-3]\,ru'+[f_l(\alpha^2r^2+1)$$
$$+\alpha^4r^4+2\alpha^2r^2-3]\,u=0, \tag{5.25}$$

where $u_1(0)=0$ and $u_1(r)$ has bounded derivatives at $r=0$,

$$u_2(a)=u_2'(a)=0, \tag{5.26}$$

and, at the interface, $r=1$,

$$u_1=u_2, \tag{5.27a}$$

$$(m-1)\,W_2'(1)\,u-(W(1)-C)\,(u_1'-u_2')=0,$$
$$u_1''+u_1'+(\alpha^2-1)\,(1-m)\,u-mu_2''-mu_2'=0,$$
$$u_1'''+2u_1''-(3\alpha^2+1)\,u_1'-mu_2'''-2mu_2''+m(3\alpha^2+1)\,u_2'$$
$$+(m-1)\,(\alpha^2-1)\,u_2+\frac{\mathrm{i}\alpha J(\alpha^2-1)}{\mathbb{R}_1(W(1)-C)}u_2=0. \tag{5.27b}$$

6. Numerical method

We used a pseudospectral method to integrate system I. This is a collocation method using Chebyshev polynomials which is particularly suited to ODE's with variable coefficients. Following Orszag & Kells (1980), we expand $(u, v, w)(r)$ in terms of

$$T_k(r) = \cos(k \arccos r), \quad k = 0, 1, 2, \ldots, N, \tag{6.1}$$

where N is a truncation number. To use this representation, we must map each of the regions occupied by the two fluids into $[-1, 1]$, $r_i \to y_i$, $i = 1, 2$,

$$r_i = \frac{(1-a_i)\, y_i + 1 + a_i}{2}, \tag{6.2}$$

$$(a_1, a_2) = (0, a). \tag{6.3}$$

The interface $r_1 = 1$ and $r_2 = 1$ maps into itself, $y_i = 1$. In each region $i = 1, 2$, we define interpolation functions of y

$$[I_N u, I_N v, I_N w] = \sum_{k=0}^{N} [\hat{u}_k, \hat{v}_k, \hat{w}_k]\, T_k(y). \tag{6.6}$$

Collocation points are

$$y_j = \cos\frac{\pi j}{N}, \quad j = 0, 1, \ldots, N, \tag{6.5}$$

where $j = N$ is a boundary point and $j = 0$ an interface point. In the core, the centreline conditions are counted as a boundary point. The interpolation functions are determined when the coefficients $(\hat{u}_k, \hat{v}_k, \hat{w}_k)$ are known. The $N+1$ coefficients $\hat{u}_k$ can be determined by $u(r_j)$ at points of collocation by requiring that

$$I_N u(y_j) = u(r_j). \tag{6.6}$$

The coefficients $\hat{v}_k$ and $\hat{w}_k$ can be obtained in the same way. We can find all the coefficients if we can determine the $3(N+1)$ values $(u, v, w)(r_j)$ at the points of collocation. The required values are generated numerically from system I. This system is to be satisfied at points of collocation. The derivatives in the differential equation at points of collocation can be expressed in terms of the functions at points of collocation through the derivative formula

$$\left.\frac{\mathrm{d}^p I_N u}{\mathrm{d}y^p}\right|_{y_k} = \sum_{j=0}^{N} u(y_j)\,(D_p)_{kj}, \tag{6.7}$$

where

$$\left.\begin{aligned}
(D_1)_{kj} &= \frac{\bar{C}_k}{\bar{C}_j}\frac{(-1)^{j+k}}{y_k - y_j}, \quad k \neq j,\\
(D_1)_{jj} &= -\frac{y_j}{2(1-y_j^2)}, \quad 1 \leqslant k = j \leqslant N-1,\\
(D_1)_{00} &= \frac{2N^2+1}{6} = -(D_1)_{NN},\\
\bar{C}_N &= \bar{C}_0 = 2,\\
\bar{C}_j &= 1, \qquad 1 \leqslant j \leqslant N-1
\end{aligned}\right\} \tag{6.8}$$

and

$$D_p = (D_1)^p.$$

There are $3(N-1)$ equations for u, v, w arising from (5.2), (5.12) and (5.13) at interior points of collocation in the annulus and $3(N-1)$ equations in the core. There are three boundary conditions at the wall, three centreline conditions in the core and six interface conditions, hence $3(N+1)$ in each region and $6(N+1)$ in all. The $6N+6$ linear equations in $6N+6$ unknowns form a linear eigenvalue problem of the type

$$(\boldsymbol{A}+c\boldsymbol{B})\cdot\boldsymbol{x}=0. \tag{6.9}$$

This eigenvalue problem was solved using the IMSL routine EIGZC.

We test for convergence by increasing the truncation number N. Converged eigenvalues $C(N)$ do not change as N is increased. There are spurious eigenvalues in the discretized system which do not converge. We find satisfactory convergence when $N \geqslant 14$.

We compared our numerical results based on collocation methods with those of JRR (1983), which are based on Galerkin methods. We find good agreement in all cases. To compare our results with theirs, we put the density ratio $\zeta_2 = \rho_2/\rho_1$ to one, $S = 0$. Their Reynolds number is Re and their complex wave speed is designated as C_{R}, related to our $\mathbb{R}_1$ and C_1 by

$$Re = \frac{a^3}{(a^2+m-1)\,m}\mathbb{R}_1, \quad C_{\mathrm{R}} = \frac{a^2+m-1}{a^2}C, \tag{6.10}$$

where $m = \mu_2/\mu_1 < 1$. The m used by JRR is $\mu_1/\mu_2 > 1$. We get agreement up to fourth-place accuracy even when the truncation number $N = 14$. The agreement is better when the azimuthal periodicity number n is small; the error is always within the bounds allowed by JRR. The results just cited imply that our results also agree with stability results for one fluid presented by Salwen & Grosch (1972) and Salwen, Cotton & Grosch (1980), which JRR (1983) reproduced.

JRR (1983) noticed some difficulties in achieving convergence at low Reynolds numbers using their Galerkin method. These problems seem not to arise when a collocation method is used.

Our numerical results for the longest waves agree perfectly with analytical results to be derived in §8. The numerical results for short waves are in agreement with those computed by Hooper & Boyd (1983, 1987) when account is taken of the difference between their problem and ours.

7. Axisymmetric and non-axisymmetric disturbances

Our numerical codes work well for non-axisymmetric as well as axisymmetric disturbances. However, we were unable to find situations in which instability definitely occurs for $n \neq 0$, with stability for $n = 0$. For this and other reasons, which we shall discuss below, we have presented results only for $n = 0$.

Some numerical results for a few discrete values of α were presented by JRR (1983) and more results by JRR (1984). In their work, density differences and surface tension are neglected and $\zeta_2 = 1$. Their computation showed that in most cases of instability with $R_1/R_2 \leqslant 0.7$, it is the axisymmetric mode which is most unstable. However, at the critical value $R_1/R_2 = 0.7$, they computed growth rates as a function of μ_1/μ_2 for $Re = 100$, $\alpha R_2 = 1$ ($\mathbb{R}_1 = 26.42, a = 1.43, \alpha = 0.7$) and found that the growth rates associated with $n = 5$ were positive and the growth rates for $n = 0$ were negative. This case then appears to be stable for $n = 0$ and unstable for $n = 5$, but appearances are illusory in the following sense. We computed growth rates corresponding to the parameters in figure 4 of JRR (1984) for $n = 5$ and $n = 0$, and

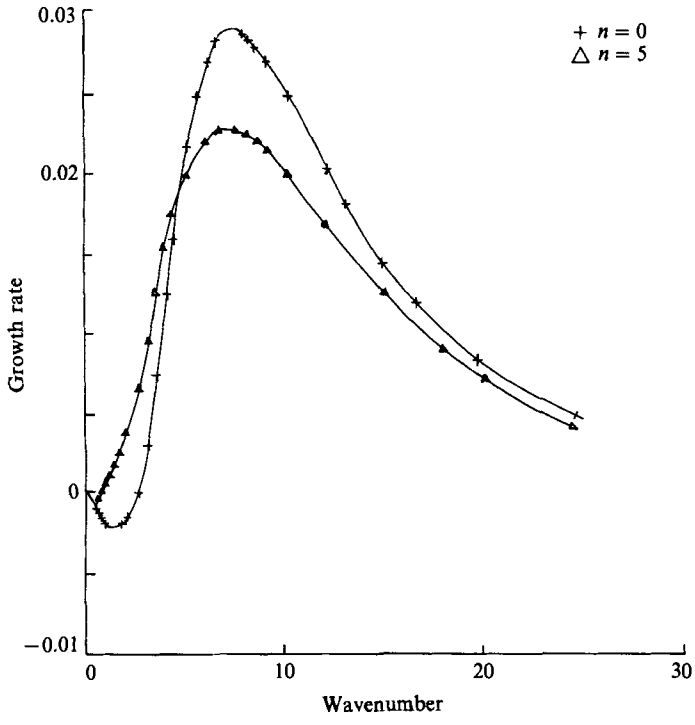

FIGURE 2. Growth rate $\alpha C_i = \alpha \operatorname{Im} C$ *vs.* wavenumber α for $a = 1.43$, $m = 0.5$, $\mathbb{R}_1 = 26.42$, $J = 0$. The addition of surface tension $J > 0$ should stabilize the curve with azimuthal wavenumber $N = 5$.

for all values of α we found that the highest growth rates are achieved for the axisymmetric mode (see figure 2). The most unstable mode for the parameters used in figure 5 of JRR (1984) is axisymmetric.

JRR (1984) also found that at any radius ratio, high azimuthal modes are unstable, but the magnitude of Im (C) decreases asymptotically with mode number. This instability of high azimuthal wavenumber and also to large α is a manifestation of the short-wave instability of Hooper & Boyd (1983) and occurs only when surface tension is zero.

We did numerical studies with different n and always found that $n = 0$ was most unstable.

There are some theoretical arguments which suggest that the axisymmetric disturbances ought to be most dangerous. The effects of surface tension appear only in the normal-stress condition (5.14) at the interface and are in the form $J(1-\alpha^2-n^2)$ where α is a positive real number and n is the azimuthal wavenumber. It is known that long waves are destabilized by surface tension; for example, there is instability even with $n = \alpha = 0$. For long-wave instability, $J(1-\alpha^2-n^2) > 0$; hence, $n = 0$ (also $\alpha < 1$). This instability, it turns out, is analogous to a capillary instability and it is axisymmetric. On the other hand, short waves are stabilized by surface tension so that waves with $n > 1$ tend to be stable: the larger n, the greater the stability. Also, the fact that Squire's theorem holds for the plane analogue of our problem (Hesla, Prankh & Preziosi 1986) shows that two-dimensional disturbances in the plane of flow are most dangerous. Hence, axisymmetric disturbances may be most dangerous even when surface tension is not important.

8. Perturbation solution for long waves

The stability problem can be solved explicitly in the limit of infinitely long waves ($\alpha \to 0$) in a power series of α using the method of Yih (1967). The axisymmetric problem can be obtained from (5.16a, c), (5.17), (5.19a), (5.20), (5.22), (5.23). The v-problem (5.16b), (5.18), (5.19b), (5.21) is decoupled and gives rise only to stable eigenvalues. Thus,

$$u(r,\alpha) = u^{(0)}(r) + \alpha u^{(1)}(r) + O(\alpha^2), \tag{8.1}$$

$$C(\alpha) = C^{(0)} + \alpha C^{(1)} + O(\alpha^2). \tag{8.2}$$

At zeroth order, we get
$$C^{(0)} = \frac{a^2(a^2-1)}{a^4+m-1}. \tag{8.3}$$

At first order,
$$C^{(1)} = \mathrm{i}\mathbb{R}_1 \frac{1-m(a^2-1)^2 G-(a^4+m-1)H}{m \quad (a^2+m-1)(a^4+m-1)}, \tag{8.4}$$

where

$$\left.\begin{aligned}
G &= -2(3a^2+2m-3)\hat{\alpha}_1 - 3(8a^2+5m-8)\beta_1 + 2(a^6+3a^2+3m-4)\hat{\alpha}_2 \\
&\quad + 3(a^8+8a^2+6m-9)\hat{\beta}_2 + (2\alpha^2+m-2)\hat{k}, \\
H &= (2a^6-3a^4+6a^2-5-12\ln a)\hat{\alpha}_2 + (3a^8-4a^6+24a^2-23-48\ln a)\hat{\beta}_2 \\
\hat{\alpha}_1 &= \frac{a^2+m-1}{a^4+m-1}\frac{m}{24}, \quad \hat{\alpha}_2 = \frac{2a^2+2m-2-ma^2}{(a^2+m-1)(a^4+m-1)}\frac{a^2}{24}, \\
\hat{\beta}_1 &= \frac{-m^2}{144(a^2+m-1)}, \quad \hat{\beta}_2 = \frac{-1}{144(a^2+m-1)}, \\
\hat{k} &= \frac{(a^2+m-1)(a^4+m-1)S}{16(1-m)} - \frac{(l-1)}{8}\frac{(a^2-1)^2(a^4+2(m-1)a^2-m+1)}{(a^2+m-1)(a^4+m-1)}.
\end{aligned}\right\} \tag{8.5}$$

To find points of the neutral curves for $\alpha = 0$, put $C^{(1)} = 0$ and solve for

$$\frac{J}{2\mathbb{R}_c^2(1-m)} =$$

$$\frac{8[(a^4+m-1)H_0-(a^2-1)^2 G_0]}{(a^2+m-1)(a^4+m-1)[(-4a^4+ma^2-3m+4)(a^2-1)+4\ln a(a^4+m-1)]}$$

$$+\frac{(\zeta_2-1)(a^2-1)[a^4+2(m-1)a^2-m+1]}{(a^2+m-1)^2(a^4+m-1)^2}, \tag{8.6}$$

where H_0 and G_0 are the same as H and G after $\hat{k}$ is put to zero.

The flow is unstable for long waves $\alpha = 0$ when

$$\frac{J^*}{a\mathbb{R}_1^2} = S > S_c = \frac{J^*}{a\mathbb{R}_c^2}. \tag{8.7}$$

The coefficent of $\zeta_2 - 1$ in (8.6) is positive whenever $a > 1$. Increasing the density of the liquid in the annulus stabilizes the flow against long waves when $m < 1$ and destabilizes when $m > 1$, but the effect is relatively weak. The effect of increasing the density of the liquid in the annulus destabilizes short waves when $m < 1$. Light lubricants are efficient against emulsification and heavy ones against capillarity.

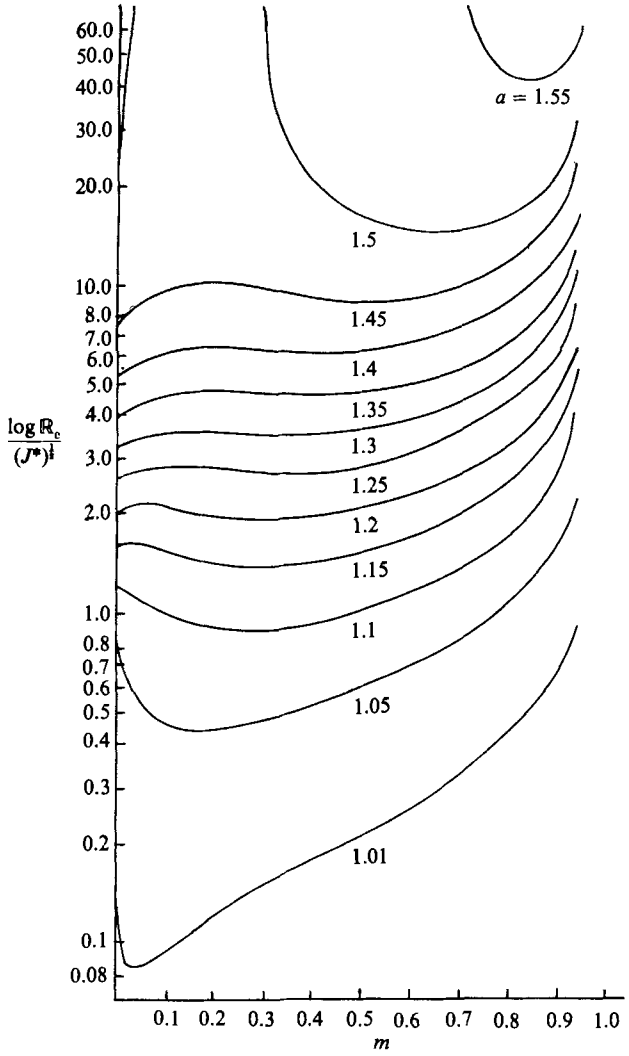

FIGURE 3. $\mathbb{R}_c/(J^*)^{\frac{1}{2}}$ as a function of m with $\alpha = 0$ and a as a parameter. The numbers on the vertical axis give values of $\mathbb{R}_c/(J^*)^{\frac{1}{2}}$.

We can write the criterion (8.7) for instability as

$$\mathbb{R}_i < \mathbb{R}_c. \tag{8.8}$$

A greater than critical amount of shearing ($\mathbb{R}_i > \mathbb{R}_c$) can stabilize capillary instabilities. It is clear that

$$S_c = f^{-1}(a, m). \tag{8.9}$$

Hence,

$$R_c^2 = J^* f(a, m)/a. \tag{8.10}$$

The lower critical Reynolds number varies with $(J^*)^{\frac{1}{2}}$. In figure 3, we show $\mathbb{R}_c/(J^*)^{\frac{1}{2}}$ as a function of m with a as a parameter. For each value of $a \leqslant 1.4889$, the values of $\mathbb{R}_c$ are finite for all $m \in [0, 1)$ and $\mathbb{R}_c \to \infty$ as $m \to 1$. When $a > 1.5805$, $\mathbb{R}_c = \infty$ for all $m \in [0, 1)$. When $1.4889 < a < 1.5805$, $\mathbb{R}_c(a, m)$ is finite for some m and is infinite for others. We may define $\hat{a}(m)$ as the a such that

$$\mathbb{R}_c(\hat{a}(m), m) \to \infty. \tag{8.11}$$

A graph of $\hat{a}(m)$ is shown as figure 4.

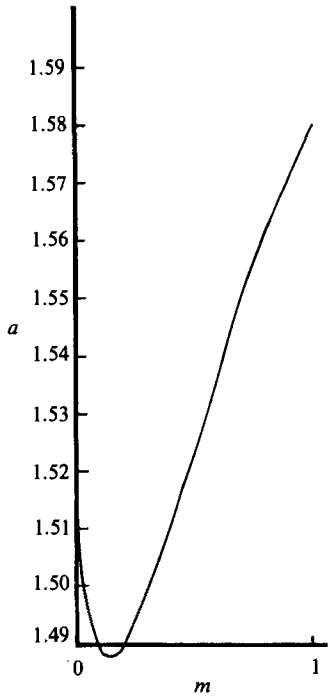

FIGURE 4. The value $\hat{a}(m)$ for which $\mathbb{R}_c(a, m) \to \infty$. At $m = 0.9999, \tilde{a} = 1.5805$. At $m = 0.15$, $\tilde{a} = 1.4889$. The region above the curve is unstable at any $\mathbb{R}$.

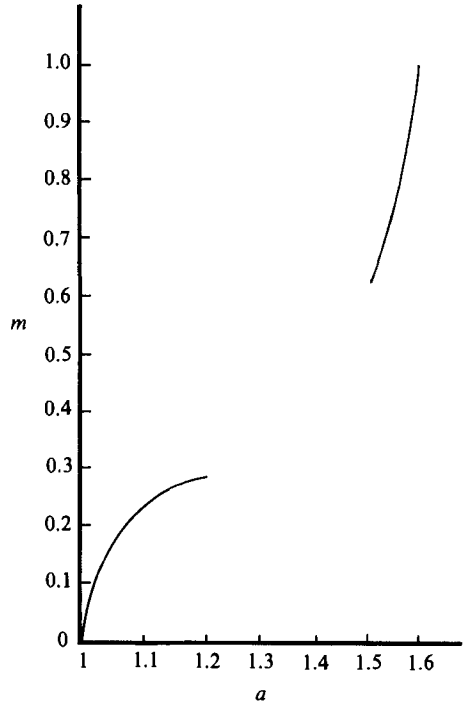

FIGURE 5. The best viscosity ratio $\hat{m}(a)$ for minimizing instability to long waves ($\alpha = 0$) according to (8.12).

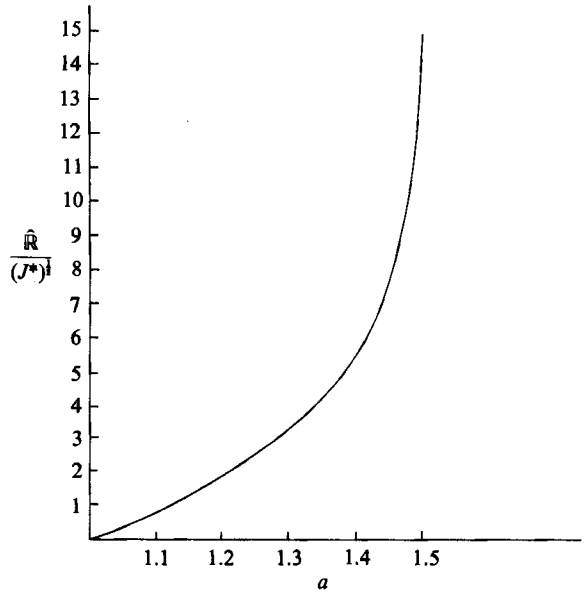

FIGURE 6. Stability limit for long waves $\alpha \to 0$ defined by (8.12). When $a = 1.5805$. $\hat{\mathbb{R}}(a) = +\infty$, and the interface will undergo a capillary instability to long waves ($\alpha \to 0$) at any $\mathbb{R}_1$. At $a = 1.55$, $\hat{\mathbb{R}}/(J^*)^{\frac{1}{2}} = 40.4$.

When $a < 1.5805$, there is a best viscosity ratio $m = \hat{m}(a)$ minimizing the region of instability to long waves:

$$\hat{\mathbb{R}}(a) = \min_{0 \leqslant m \leqslant 1} \mathbb{R}_c(a, m) = \mathbb{R}_c(a, \hat{m}(a)). \tag{8.12}$$

The graph of $\hat{m}(a)$ is shown in figure 5 and the graph $\hat{\mathbb{R}}(a)$ in figure 6.

The solution just derived sets a correct standard for testing our pseudospectral numerical method. In all cases, we get four-place accuracy from the numerical method truncated at $N = 14$.

9. Comparison with results of Hooper & Boyd

Hooper & Boyd (1983) have considered the linear theory of stability of an unbounded plane Couette flow with constant shear rates above and below a flat interface matched so that the shear stress is continuous. Their analysis is relevant locally in the limit of short waves, $\alpha \to \infty$, and it predicts universal instability in all cases in which surface tension vanishes. Surface tension can be included in their analysis for S small enough that

$$\alpha^3 S \leqslant O(1) \tag{9.1}$$

as $\alpha \to \infty$. Surface tension stabilizes the short-wave instability.

Renardy (1985) did a numerical study of plane Couette flow of two superposed liquids between parallel walls, and she found an instability which did not reduce to that of Yih (1967) as $\alpha \to 0$ or to that of Hooper & Boyd (1983). Hooper & Boyd (1987, hereinafter referred to as HB 1987) studied Renardy's finite-α instability for shear flow of two fluids in a semi-infinite region above a flat plate using an asymptotic method and also a numerical evaluation of the secular equation arising

from an Orr–Sommerfeld type of analysis, using Airy functions. They characterized the α interval for the finite-α instability as

$$\left(\frac{\alpha_{HB}^2}{\mathbb{R}_{HB}}\right)^{\frac{1}{3}} \ll 1, \quad (\alpha_{HB}\,\mathbb{R}_{HB})^{\frac{1}{3}} \gg 1. \tag{9.2}$$

Basically, this is a large R_{HB} instability.

The problem of HB (1987) looks locally like core–annular flow when the lubricating layer in the annulus is thin. However, the two problems are not comparable because of the effect of the curvature terms, which are probably of secondary interest, and because their plane problem does not admit capillary instability. The first term in the surface-tension expression $S(1-\alpha^2)$ is responsible for instability to long waves and it is absent in the plane problem. Surface tension in HB's problem appears as $-S\alpha^2$ and can only stabilize short waves.

Useful formulas for frequencies and growth rates were derived by HB (1987), and they were able to identify the new instability with the viscous boundary layer at the wall. They note, however, that their asymptotic results are not uniform in the viscosity ratio μ_1/μ_2 and they fail in the limit $\mu_1/\mu_2 \to \infty$ which is of interest for lubricated pipelining (cf. §10 of this paper).

In figure 7, we superimposed the results of our pseudospectral code on the numerical results computed by HB and exhibited as figure 5 of their paper. The comparison requires that we identify the constant shears which represent the parabolic arcs of core–annular flow. When $\alpha \gg 1$ and $S = 0$, the instability is local in the sense of HB (1983). For this limit the choice of the local rate of shear at the interface is obligatory.

There are some discrepancies between our results and HB (1987), as can be seen from figure 7. To facilitate the explanation of these discrepancies, we shall need a list of conversion factors. We attach the subscript HB to the symbols used by HB (1987).

$$\left.\begin{aligned} \mathbb{R}_{HB} &= \frac{2(a-1)^2}{m(a^2+m-1)}\mathbb{R}, \quad \mathbb{R} = \mathbb{R}_1, \\ S_{HB} &= \frac{(a^2+m-1)^2}{4(a-1)^3}S, \\ m_{HB} &= 1/m, \\ \alpha_{HB} &= (a-1)\,\alpha, \\ \frac{C_{HB}}{\mathbb{R}_{HB}} &= \frac{m(a^2+m-1)}{4(a-1)^3}\frac{C}{\mathbb{R}}. \end{aligned}\right\} \tag{9.3}$$

Figure 7 is identical to figure 5 in HB (1987) except for the dots, crosses and squares which are values computed from our numerical program. The notation on figure 7 is as originally presented by HB (1987) except that we have assigned a subscript HB to all the symbols.

The vertical bars on the curves $S_{HB} = 0.1$ and $S_{HB} = 0.00498$ are at $\alpha_{HB}^3 S_{HB} = 1$. Given the difference between our problem and HB's problem the comparison for $\alpha_{HB}^3 S_{HB} < 1$ suggests agreement. The difference between our results and those of HB vanish for large α_{HB} when $S_{HB} = 0$. There is disagreement for large α_{HB} when $\alpha_{HB}^3 S_{HB} > 1$ because the curves marked $S_{HB} = 0.00498$ and $S_{HB} = 0.1$ are computed from the short-wave formula given in the caption, which was derived in HB (1983),

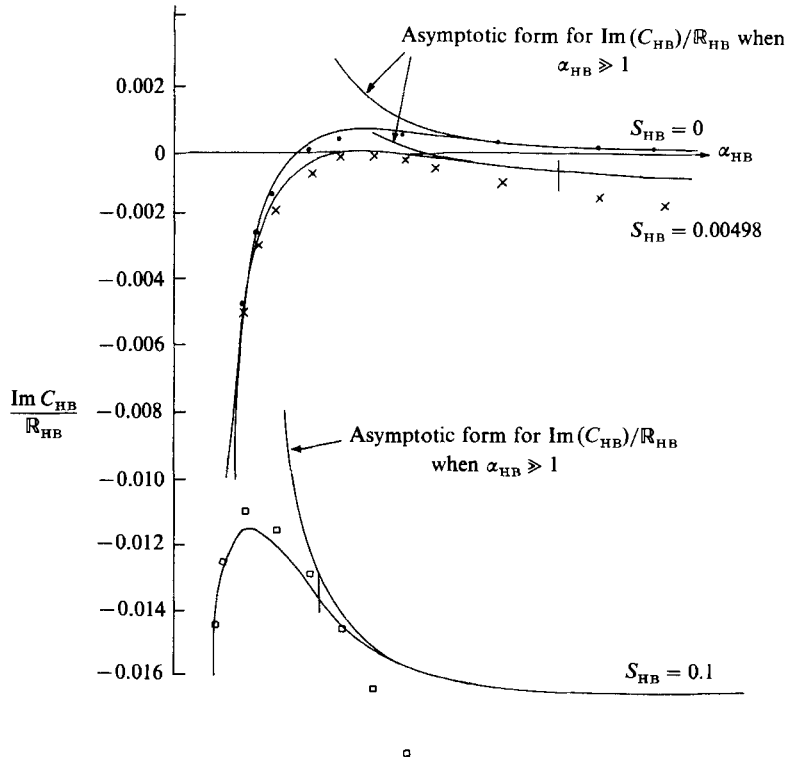

FIGURE 7. (After Hooper & Boyd 1987) $\mathrm{Im}\, C_{HB}/\mathbb{R}_{HB}$ *vs.* α_{HB} when $m_{HB} = 2$ and $\beta_{HB} \gg 1$ for different values of S_{HB}. The upper branch shown at each value of S_{HB} is the asymptotic form for $\mathrm{Im}\, C_{HB}/\mathbb{R}_{HB}$, which is

$$\frac{1}{2(1+m_{HB})\alpha_{HB}^3}\left[\left(\frac{1-m_{HB}}{m_{HB}}\right)^2 - \alpha_{HB}^3 S_{HB}\right].$$

The dots, crosses and squares are points computed from our pseudospectral code for CAF. See text for explanation.

and the formula is not valid when $\alpha_{HB}^3 S_{HB} > 1$. Evidently surface tension is much more stabilizing for short waves than is indicated by the asymptotic results of HB (1983).

10. $m \to 0$ for $\mathbb{R}_1 \neq 0$ is a singular limit

We have already mentioned that $m = 0$ is an important limit for lubricated pipelining. Since $m = \mu_2/\mu_1$, we get very small m when lubricating viscous crudes $\mu_1 = 1000$ P with water $\mu_2 = 1/100$ P, $m = 10^{-5}$.

Consider the axisymmetric problem (5.25), (5.26) and (5.27). The Reynolds number for the water $\mathbb{R}_2$ appears only in the water equation (5.25) when $1 \leqslant r \leqslant a$ and $\mathbb{R}_2 = \mathbb{R}_1/m$. If $\mathbb{R}_1 \neq 0$ and $m \to 0$, the water equation is inviscid,

$$r^4 u_2'' - r^3 u_2' + (\alpha^2 r^2 + 1) r^2 u_2 = 0, \tag{10.1}$$

two derivatives are lost. To solve this singular perturbation problem at zeroth order, it is necessary to discard certain boundary and interface conditions. The no-slip

condition $u_2'(a) = 0$ and (5.27b) are set aside. The shear-stress condition (5.22) reduces to

$$u_1''' + u_1' + (\alpha^2 - 1)\, u_1 = 0, \tag{10.2}$$

which is an uncoupled condition on u_1. On the other hand, (5.23) reduces to

$$u_1''' + 2u_1'' - (f_1 + 3\alpha^2 + 1)\, u_1' + f_1 \zeta_2 u_2' + \{f_1(\zeta_2 - 1) - \mathrm{i}\alpha \mathbb{R}_1 W_2'(1)\, \zeta_2 + 1 - \alpha^2\}\, u_1 + \frac{\mathrm{i}\alpha J(\alpha^2 - 1)}{\mathbb{R}_1(W(1) - C)} = 0, \tag{10.3}$$

whereas (5.24) reduces to

$$u_1''' + 2u_1'' - (3\alpha^2 + 1)\, u_1' + f_1(\zeta_2 - 1)\, u_2' + \{f_1(\zeta_2 - 1) - \mathrm{i}\alpha \mathbb{R}_1(\zeta_2 - 1)\, W_2'(1) + 1 - \alpha^2\}\, u_1 + \frac{\mathrm{i}\alpha J(\alpha^2 - 1)\, u_1}{\mathbb{R}_1(W(1) - C)} = 0. \tag{10.4}$$

These two equations couple the flow in the water to the flow in the oil through terms proportional to u_2'. Equations (10.3) and (10.4) are equivalent when (5.27b) holds. If (5.27b) is discarded *ab initio*, we are obliged to use (10.3). This is the form of the normal stress when the outer fluid is regarded as inviscid from the start and the continuity of the axial component of velocity (3.5), which leads to (5.27b), is omitted.

Equation (10.3) decouples from the water when $\zeta_2 = 0$. Then (5.25), (10.2) and (10.3) are enough to determine the family of eigenvalues given by Chandrasekhar (1961) in his study of capillary instability of a viscous jet. To identify our problem with his, we note that when $m = 0, W_1(r) = 1$. Then put $\mathbb{R}_1(1 - C) = \hat{C}$, which is equivalent to rescaling the time. To complete the formal identification of this problem with Chandrasekhar's, put $W_0 = \nu/R_1$. In dimensionless variables, Chandrasekhar's problem can be written as

$$\boldsymbol{u}_t = -\nabla p/\rho + \nabla^2 \boldsymbol{u} \quad \text{on} \quad 0 \leqslant r \leqslant 1$$

with $\quad u = \delta_t, \quad u_x + w_r = 0, \quad -p/\rho + 2u_r = J(\delta_{\theta\theta} + \delta_{xx} + \delta) \quad \text{on} \quad r = 1.$

It follows that $\hat{C}$ depends on a wavenumber α and the surface-tension parameter J. The limit $\nu \to 0, J \to \infty$ corresponds to an inviscid jet, leading to Rayleigh's theory with maximum growth rate at $\tilde{\alpha} = 0.697$. The wavenumber $\tilde{\alpha}(J), 0 \leqslant \tilde{\alpha} \leqslant 1$ which maximizes $\sigma = \alpha \hat{C}(\alpha, J)$ is an increasing function with $\tilde{\alpha}(\infty) = 0.697$. For small J, Chandrasekhar (1961) showed that to a good approximation $\sigma = T(1 - \alpha^2)/6\mu_1 R_1$, hence, $\tilde{\alpha}(0) = 0$. Small J corresponds to situations in which viscosity is paramount. The most dangerous wave for very viscous jets is very long.

11. The limit $\mathbb{R}_1 \to 0$ and $m \neq 0$

This is not a singular limit, $\mathbb{R}_2 = \mathbb{R}_1/m$ tends to zero with $\mathbb{R}_1$ and we get Stokes linearized equations in the oil and in the water. It is again appropriate to calculate eigenvalue $C = \hat{C}/\mathbb{R}_1$. Then, when $\mathbb{R}_1 \to 0$, $f_1 = -\mathrm{i}\alpha \hat{C}$ and $f_2 = -\mathrm{i}\alpha \hat{C}/m$, (5.27$b$) reduces to

$$u_1' = u_2' \quad \text{at} \quad r = 1$$

and the last term of (5.27b) is replaced by

$$-\mathrm{i}\alpha J(\alpha^2 - 1)\, u_2/\hat{C}.$$

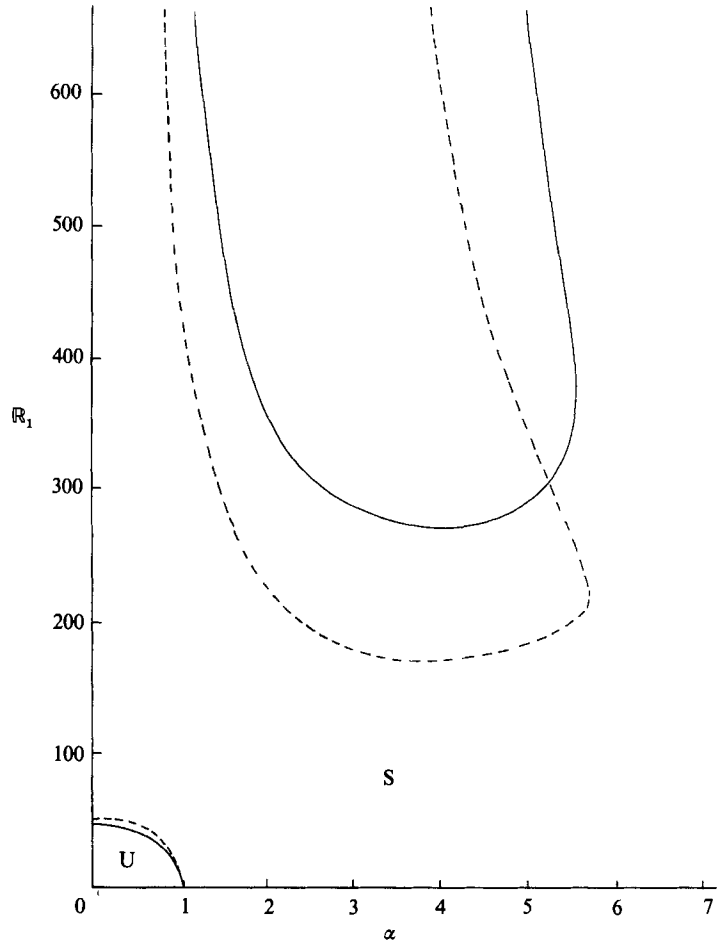

FIGURE 8. Neutral curves $\mathbb{R}_c(a, m, J^*)$, $J^* = 930$, $a = 1.15$, $m = 0.05$ (– – –); $m = 0.1$ (——). The band of Reynolds numbers between the upper and lower critical branches is stable.

This problem is independent of $\mathbb{R}_1$ and also of $W_l(r), l = 1, 2$, as it should be in the Stokes' flow limit.

Surface tension J is stabilizing when $\alpha > 1$ and destabilizing when $\alpha < 1$. In all cases for which $\mathbb{R}_1 \to 0$, we found core–annular flow (CAF) to be stable when $\alpha > 1$ and unstable when $\alpha < 1$. This is shown clearly in figure 12 and in the neutral curves exhibited in §§12 and 13. Values of $\tilde{\alpha}(a, m, J)$ of the fastest growing wave show that the Stokes' flow limit $\mathbb{R}_1 \to 0$ depends on a, m, J. We recover the capillary instability of Chandrasekhar (1961) numerically by fixing $m \ll \mathbb{R}_1 \to 0$, and the capillary instability of Rayleigh (1879) by putting $J \to \infty$ when m/R_1 is small and $\mathbb{R}_1 \to 0$.

12. Neutral curves

There are many different types of neutral curves. We have computed some representative types, shown in figures 8–10, and 12–16. The results given in §13 are a fairly complete representation of what linear theory has to say about the results described in figure 1.

Figure 8 shows a fairly representative situation, with disjoint neutral curves, an

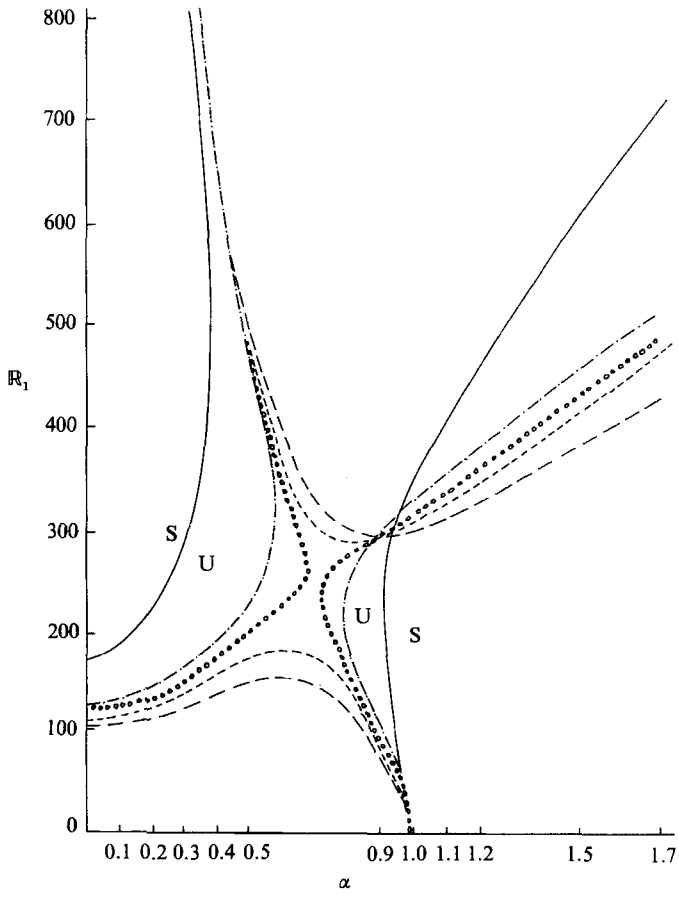

FIGURE 9. Neutral curves $\mathbb{R}_c(a, m, J^*)$, $J^* = 930$, $a = 1.25$, $m = 0.9$ (——); $m = 0.8$ (—·—·—); $m = 0.78$ (○○○○); $m = 0.75$ (- - - -); $m = 0.7$ (– – –). The stable band of Reynolds numbers disappears between $m = 0.78$ and $m = 0.75$.

upper and lower branch. The lower branch is associated with long waves leading to capillary instability caused by surface tension at low Reynolds numbers. This region is in the bottom left-hand corner of the $(\alpha, \mathbb{R}_1)$-plane. It terminates on $\alpha = 1$ for $\mathbb{R}_1 = 0$. The values $\mathbb{R}_1 = \mathbb{R}_c$ as a function of a and m when $\alpha = 0$ were given in §8. When $a > 1.5805$, disturbances with $\alpha = 0$ are unstable at all $\mathbb{R}$. We may define a critical stability limit for the lower branch:

$$\tilde{\mathbb{R}}_L(a, m, J^*) = \max_{\alpha \geq 0} \mathbb{R}_{cL}(a, m, J^*, \alpha). \tag{12.1}$$

The flow is unstable to generalized capillary instability when $\mathbb{R}_1 < \mathbb{R}_L$.

The upper branch of the neutral curve is associated with larger α, shorter waves and larger Reynolds number. We may define a critical stability limit for the upper branch:

$$\tilde{\mathbb{R}}_U(a, m, J^*) = \min_{\alpha \geq 0} \mathbb{R}_{cU}(a, m, J^*, \alpha). \tag{12.2}$$

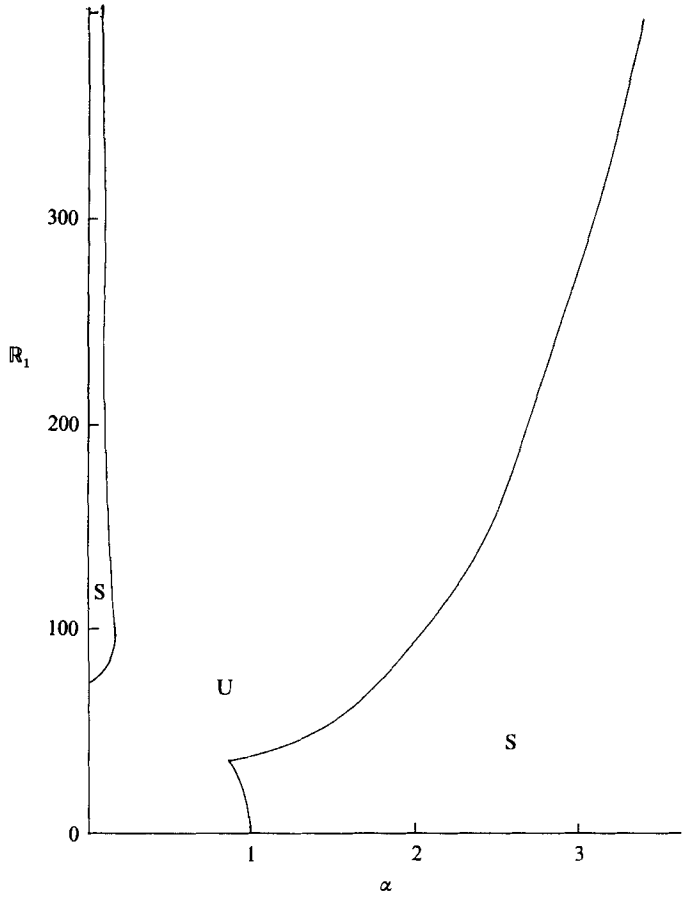

FIGURE 10. Neutral curves $\mathbb{R}_c(a, m, J^*)$, $J^* = 930$, $a = 1.25$, $m = 0.01$. The lower critical condition and upper critical condition have merged. Stable CAF is not possible.

Core–annular flow (CAF) is unstable, evidently leading to emulsions when

$$\mathbb{R}_1 > \tilde{\mathbb{R}}_U.$$

When

$$\tilde{\mathbb{R}}_L < \mathbb{R}_1 < \tilde{\mathbb{R}}_U \tag{12.3}$$

we have stable CAF.

The topology of the neutral curves can change with parameters. This is shown clearly in figure 9 which shows a change of topology leading to destruction of the upper and lower branches and the formation of left and right neutral branches for $J^* = 930, a = 1.25$ for some m between 0.75 and 0.78. Left and right branches of the neutral curve R_c is also shown in figure 10.

In figure 11, we have given a graphical representation of (12.3) for $J^* = 930, a = 1.25$ for different values of m. CAF is stable in the enclosed region of the figure.

Figure 12 shows that increasing J^* stabilizes short waves $\alpha > 1$ and destabilizes long ones $\alpha < 1$.

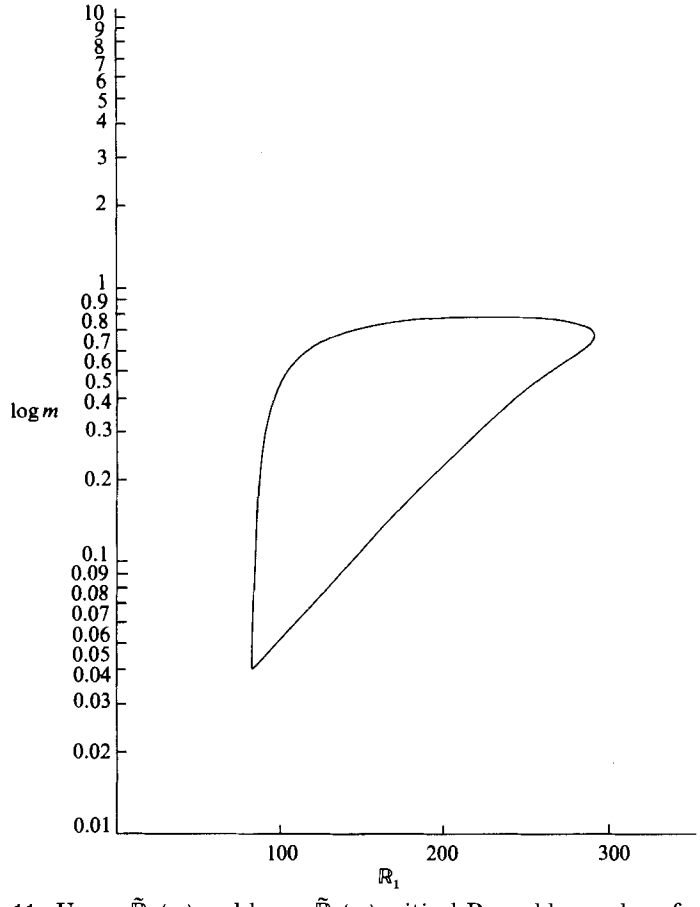

FIGURE 11. Upper $\tilde{\mathbb{R}}_U(m)$ and lower $\tilde{\mathbb{R}}_L(m)$ critical Reynolds numbers for $a = 1.25$ and $J^* = 930$. Core–annular flow is stable in the enclosed region.

13. Comparison with experiments

Now we shall compare the results of experiments of CGH (1961) with predictions of eigenvalues of the linear theory of stability. In their paper, they presented pictures of the flow in eleven different cases. These pictures are exhibited in figure 1. We have calculated neutral curves and growth rates for these eleven experiments. The neutral curves are exhibited in figures 13–16 and the growth rates for the fastest growing wave are listed in table 1.

(1) We used linear theory to predict the windows of operating parameters for stable CAF.

(2) We used the neutral curves to identify the nature of the instability that should be observed in the experiments. We aim to discriminate between conditions in which they got bubbles and slugs of oil in water from those in which they got emulsions of water in oil.

(3) We used the calculation of the length of the most rapidly growing wave to predict the length of slugs and bubbles that should arise from the capillary instability.

In all eleven experiments, except Experiment 2, CAF is unstable in the experiments and in the theory. In principle there is no reason why the flow observed under

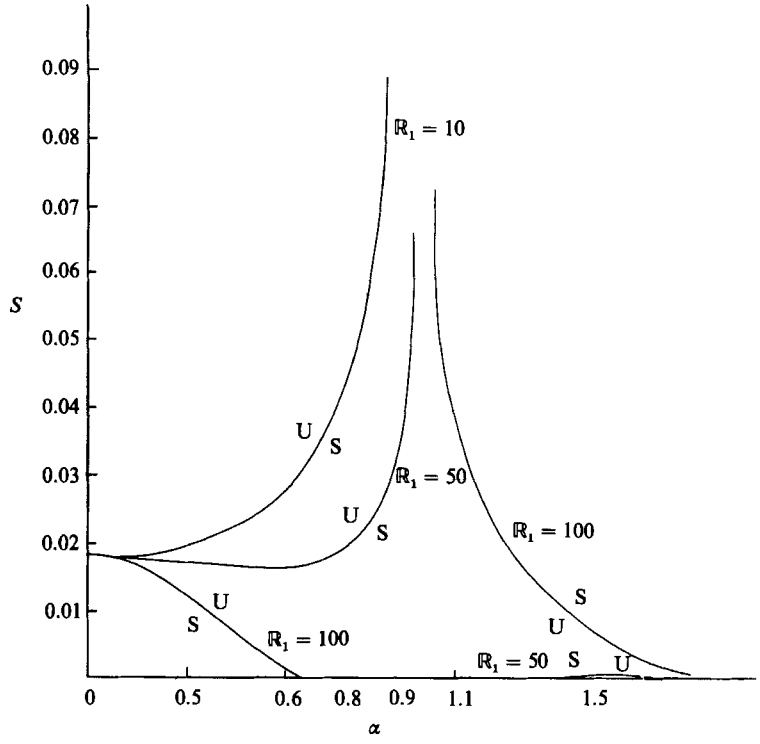

FIGURE 12. Neutral curves in the (α, S)-plane for $a = 1.4$, $m = 0.5$. Increasing S at a fixed $\mathbb{R}_1$ is the same as increasing J. Increasing J at fixed α and $\mathbb{R}_c$ destabilizes long waves ($\alpha < 1$) and stabilizes short waves ($\alpha > 1$).

	Experiment			Theory		
#	a	R_1	l_{exp}	$\tilde{\alpha}$	$\sigma(\tilde{\alpha})$	l
3	1.42	69.80	4.5 (short slug) 7.5 (long slug)	0.6	$7.835\,18 \times 10^{-2}$	5.2665
4	2.24	26.98	0.85 (bubble)	0.66	$2.916\,16 \times 10^{-1}$	0.8596
6	1.5	406.90	> 15.75 (slug)	0.22	$5.859\,69 \times 10^{-3}$	12.1856
7	1.74	287.41	13.1 (slug)	0.08	$2.346\,65 \times 10^{-3}$	21.4686
8	2.80	134.50	0.69 (middle-most bubble)	0.61	$5.238\,81 \times 10^{-2}$	0.7060
9	1.81	795.97	6.0 or > 15.75 (slug)	0.32	$6.840\,2 \times 10^{-2}$	4.7682
				0.023	$5.398\,95 \times 10^{-4}$	66.3405
10	2.65	433.70	2.70 (longest slug)	0.11	$1.827\,20 \times 10^{-2}$	4.4199
11	4.63	221.69	0.3125 (largest bubble)	0.64	$2.414\,83 \times 10^{-2}$	0.4202

TABLE 1. Comparison of theory and experiment. The # refers to pictures shown in figure 1. $\sigma(\alpha) = \alpha C_i(\alpha)$ is the growth rate and $\tilde{\alpha}$ is the wavenumber of the fastest growing wave. lR_2 is the length of a slug or the radius of a bubble.

unstable conditions should correlate with the predictions of a linear theory. The bubbles, slugs and emulsions seen in the experiments are not small perturbations of CAF. Nevertheless, the predictions of the linear theory do seem to correlate with observations.

To apply the results of our stability calculation to the experiments, we need to

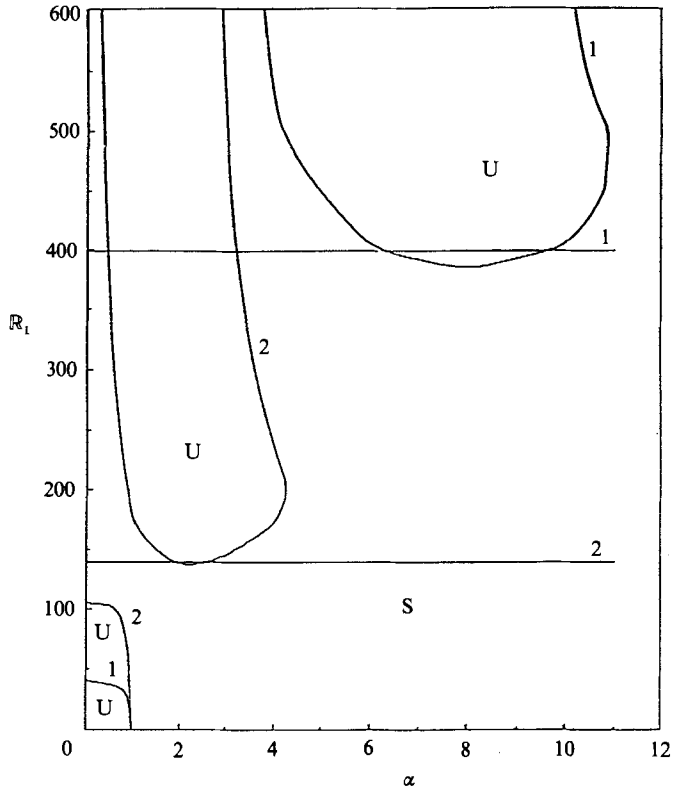

FIGURE 13. Neutral curves corresponding to Experiments 1, 2: $a = 1.08, 1.21$; $J^* = 2102$; $m = 0.0532$. The horizontal lines correspond to the Reynolds number of the experiments. For Experiment 2, the minimum value $\mathbb{R}_1 = 138.2$. Stable core–annular flow is observed with $\mathbb{R}_1 = 138.6$. The maximum growth rate $\hat{\alpha}c_1(\hat{\alpha}) = 2.747 \times 10^{-3}$ occurs at $\alpha = \hat{\alpha} = 2.24$. This flow is almost stable.

convert data given in the experiment into parameters used in the analysis. The superficial velocities are the volume flow rate divided by the area of the pipe. From these flow rates and the values of material parameters, we may compute R_1 and W_0 for stable CAF. This fixes all of the dimensional, hence, dimensionless, parameters used in the analysis. The solution is carried out in c.g.s. units. The viscosity of water is given as 0.984 cP. For the oil viscosity (16.8 cP) listed in figure 1, we get $m = 0.0532$. Carbon tetrachloride was added to the oil to increase the oil density. The density was matched, $\zeta_2 = 1$. The interfacial tension between the 16.8 cP oil and water was measured by the method of capillary rise and is given as 45 dyne/cm. (The capillary rise method is not accurate and the evaporation of carbon tetrachloride makes it likely that the surface tension value is not accurate and could have changed by as much as 5 dynes/cm from experiment to experiment.) In all the cases exhibited in figure 1, water wets the wall of the cellulose acetate-butyrate. Let W_{1s} be the superficial velocity of the oil (called V, in figure 1) and W_{2s} the superficial velocity of water with $\xi = W_{1s}/W_{2s}$ from (2.8) and

$$a = \left\{\frac{1+\xi+(1+m\xi)^{\frac{1}{2}}}{\xi}\right\}^{\frac{1}{2}}, \quad W_0 = \frac{2W_{2s}}{m}(1+m\xi)^{\frac{1}{2}}[m-1+(1+m\xi)^{\frac{1}{2}}]. \tag{13.1}$$

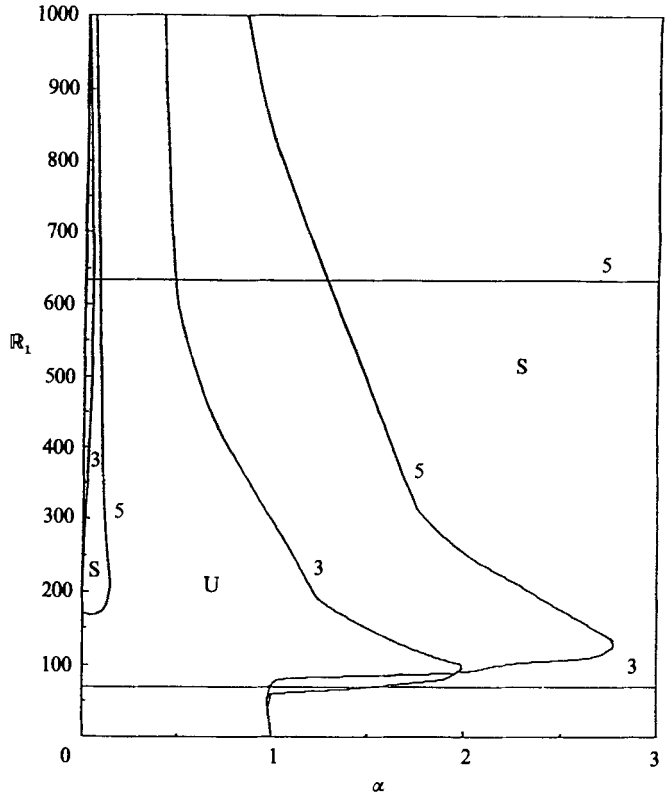

FIGURE 14. Neutral curves corresponding to Experiments 3, 5: $a = 1.42, 1.31$; $J^* = 2102$; $m = 0.0532$. Oil slugs in water are observed in Experiment 3. Water drops in oil are observed in Experiment 5.

Then,

$$\left.\begin{aligned} \mathbb{R}_1 &= \frac{\rho_1 W_0 R_1}{\mu_1} = \frac{\rho_1 W_0 R_2}{a\mu_1}, \\ S &= \frac{T}{\rho_1 R_1 W_0^2} = \frac{aT}{\rho_1 R_2 W_0^2} = \frac{J^*}{a\mathbb{R}_1^2}. \end{aligned}\right\} \tag{13.2}$$

The values of the superficial velocities are given in figure 1.

The comparisons between theory and experiments are made in figures 13–16 (in which the neutral curves corresponding to the 11 drawings shown in figure 1 are exhibited) and in table 1. The table gives the wavelength $\alpha = \tilde{\alpha}$ corresponding to the maximum growth rate

$$\tilde{\alpha} C_i(\tilde{\alpha}) = \max_{\alpha \geqslant 0} \operatorname{Im} \alpha C(\alpha). \tag{13.3}$$

The dimensionless wavelength corresponding to $\tilde{\alpha}$ is $\tilde{\lambda} = 2\pi/\tilde{\alpha}$ and the dimensional one is $\tilde{\lambda} R_1$.

The window of parameters for stable CAF may be expressed as an interval

$$\tilde{\mathbb{R}}_L < \mathbb{R}_1 < \tilde{\mathbb{R}}_U \tag{13.4}$$

between the maximum $\mathbb{R}_1$ on the lower branch of the neutral branch and the minimum $\mathbb{R}_1$ on the upper branch. Such an interval exists when the lubricating layer is small but not when it is large. Recall that the flow is always unstable to long waves

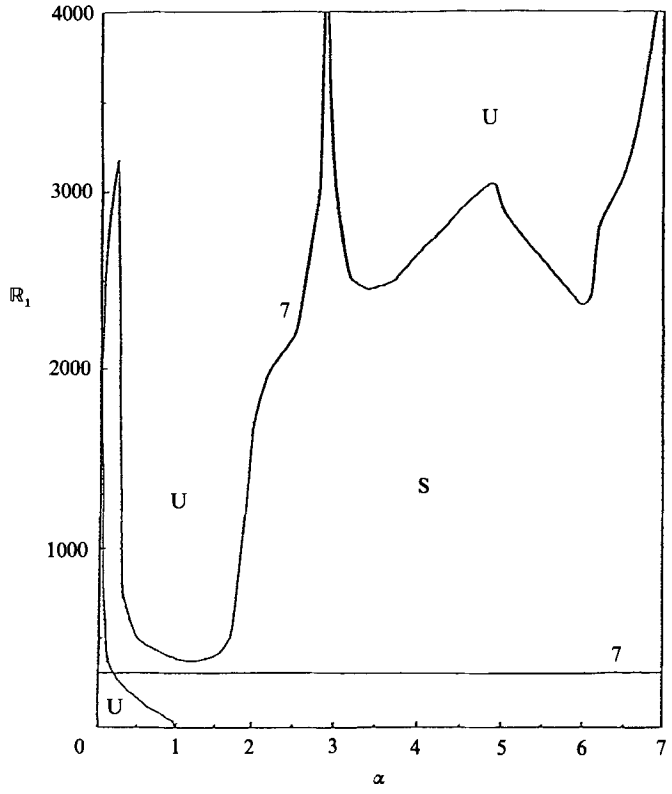

FIGURE 15. Neutral curves corresponding to Experiment 7: $a = 1.74$, $J^* = 2102$, $m = 0.0532$. Oil slugs in water are observed. For Experiments 9, 4, 10, 8, 11 ($a = 1.84, 2.24, 2.65, 2.80, 4.63$, respectively) the neutral curves are very similar to the one shown here except for some scale changes. These other neutral curves are available from the authors on request.

$\alpha \to 0$ when $a > 1.5805$. The minimum $\mathbb{R}_U$ decreases rapidly as a is increased. We may describe this result in terms of a critical Reynolds number

$$Re = \frac{(R_2 - R_1)\, W_0}{\nu_1} = \frac{\tilde{\mathbb{R}}_U (a-1)}{m}$$

in the lubricating layer. The numerical results show that Re is a rather weak function of a and $Re \approx 660$. Hence, we get a weak approximation

$$\tilde{\mathbb{R}}_U \approx \frac{m660}{(a-1)} = \frac{35.21}{a-1}.$$

On the other hand, the maximum value $\tilde{\mathbb{R}}_L$ on the lower critical branch is an increasing function of $a-1$ (see figure 6). Hence, as a increases, the interval (13.4) shrinks; and the construction implied by the foregoing argument, shown in figure 17, indicates that CAF is always unstable under the experimental conditions ($m = 0.0532, J^* = 2102$) of the experiments of CGH when $a > a_c$, where $a_c \approx 1.23$. The same argument shows that CAF is more stable when the lubricating is thinner with maximal intervals (13.4) of stability as $a \to 1$.

CGH observed stable CAF in Experiment 2 and only in Experiment 2. The theoretical result for this experiment is shown in figure 13. The experiment lies very

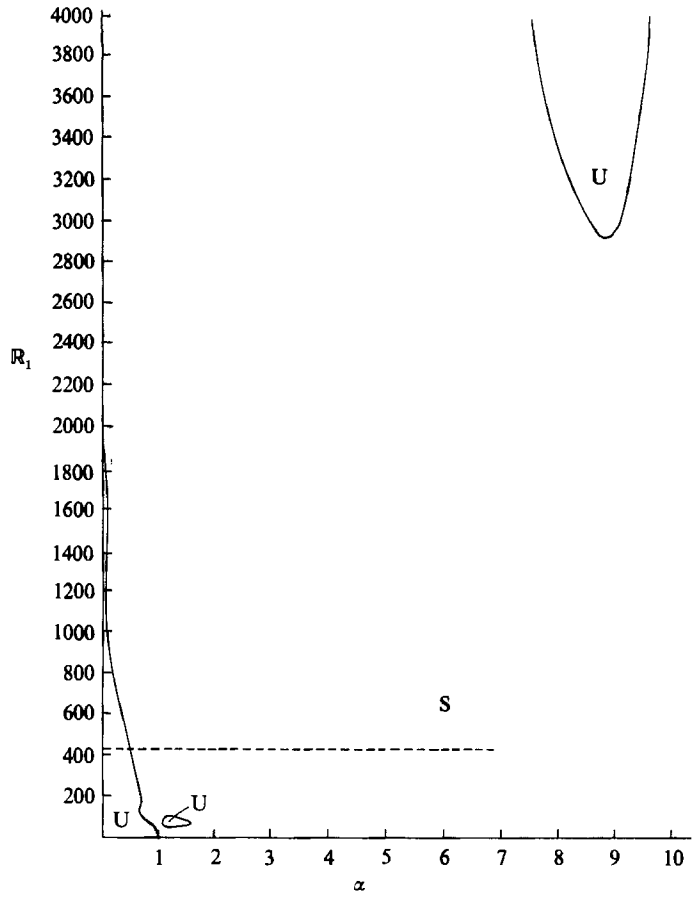

FIGURE 16. Neutral curves corresponding to Experiment 6: $a = 1.50$, $J^* = 2102$, $m = 0.0532$. CAF plus water drops in oil are observed at $\mathbb{R}_1 = 40.7$

nearly in the stable band of Reynolds numbers with a weak short-wave instability (cf. growth rates, figure 13) in a narrow interval centred on $\alpha = 2.2$. Very minor adjustments of the values of operating parameters, well within the errors expected of these experiments, would place the flow entirely within the stable band. All the other ten cases are unstable in the experiments and in the theory.

We next consider category (2) of the comparison between theory and experiment. There are two cases and only two cases of emulsification of water into oil, shown in figure 1 as experiments 1 and 5, with associated neutral curves in figures 13 and 14. In both cases, we get an instability for high Reynolds number $R_1 > \tilde{\mathbb{R}}_U$ above the upper critical, short-wave branch.

The flows in all the other experiments (3, 4, 6, 7, 8, 9, 10, 11) shown in figure 1 are unstable and the theory, exhibited in figures 14–16, show that the instability is to long waves and not to short waves. For these long-wave instabilities, there is always a wavelength $\tilde{\lambda} = 2\pi/\tilde{\alpha}$ which maximizes the rate of growth (13.3) of an unstable wave. The length of slugs and bubbles of oil in water, shown in figure 1, can be compared with a theoretical value we get from computing $\tilde{\alpha}$. The procedure we use is to identify the volume of a cylinder

$$\pi R_1^2(\tilde{\lambda} R_1) = \frac{2\pi^2}{\tilde{\alpha}} R_1^3 \tag{13.5}$$

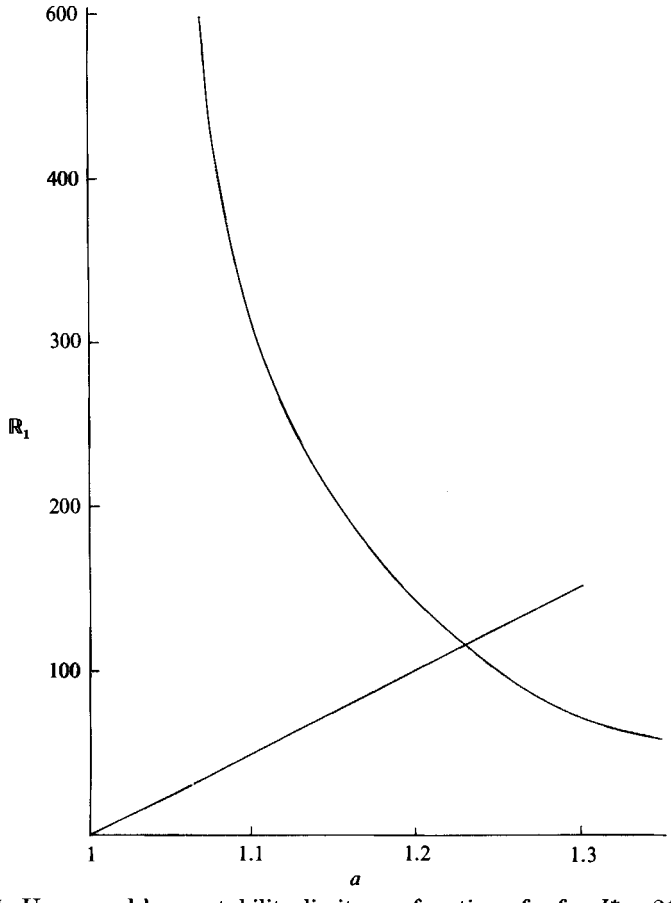

FIGURE 17. Upper and lower stability limit as a function of a for $J^* = 2102$, $m = 0.0532$. CAF is never stable when a is larger than $a \approx 1.23$ at the point of intersection.

of radius R_1 and length $\tilde{\lambda}R_1$. We say that this volume is preserved in the nonlinear breakup of the oil, hence, is the same as the volume of slugs and bubbles observed in the experiments. (The words 'oil drops' used by CGH in Experiment 11 is a misnomer. Small oil bubbles are shown there.) If $\tilde{\alpha}$ is very small, then the wavelength is many times the circumference of the core. The oil in such a long wave can gather together to form something like a spherical bubble only if the pipe is large enough. Otherwise the bubble cannot collect into a closed spherical shape; it takes form as a cylinder, perhaps long, which we call slug. Slugs and bubbles, like CAF, seem well lubricated by water at a radius something like $a \approx 1.20$, as in Experiments 3, 6, 7 and 9. Hence, $R \approx R_2/1.20$ and the volume (13.5) is equal to volume of the observed slug with area $\pi(R_2/1.2)^2$ and length lR_2,

$$\pi\left(\frac{R_2}{1.2}\right)^2 (lR_2) = \frac{2\pi^2}{\tilde{\alpha}} R_1^3. \tag{13.6}$$

Hence
$$l = 1.44\tilde{\lambda}/a^3 = 2.88\pi/\tilde{\alpha}a^3. \tag{13.7}$$

The volume of observed bubbles is $\frac{4}{3}\pi b^3$. Equating this to (13.5), we define

$$l = \frac{b}{R_2} = \left(\frac{3\pi}{2\tilde{\alpha}}\right)^{\frac{1}{3}} \frac{1}{a}. \tag{13.8}$$

We measured the length $l_{\exp} R_2$ of observed slugs from the pictures in figure 1. The $l_{\exp}$ give the number of pipe radii in the length of one slug and it can be compared with the l in (3.17). An identical measurement of the ratio of the bubble radius b to R_2 determines an $l_{\exp}$ to compare with theoretical ratio in (13.8).

Theory and experiment are compared in table 1, where we have identified the experiments by the numbers shown in figure 1. In the table, we list the value $\mathbb{R}_1$, the wavenumber $\tilde{\alpha}$ of the fastest growing wave, the growth rate $\tilde{\sigma} = \tilde{\alpha} C_i(\tilde{\alpha})$ of this wave, the theoretical value l from (13.7) (for Experiments 3, 6, 7, 9 and 10) or (13.8) (for Experiments 4, 8 and 11) and the measured value $l_{\exp}$. The size of bubbles and slugs that can be observed in figure 1 under any particular operating condition is not unique. Since we compute a unique size based on the assumption of constant volumes, our comparison is only suggestive and not precise. Some remarks about the comparisons shown in table 2 are necessary. In the table, we have identified which slug or bubble has been used for comparison. We do not know if the size of slugs and bubbles, so identified, is representative. For example, there may be a longer or shorter slug upstream or downstream of the section showing the single long slug exhibited in Experiment 7 of figure 1. In some of the experiments, like 6, 9 and 10, there is a great variability with different sizes and configuration occurring simultaneously. Only Experiment 2 of the three labelled 'oil in water concentric' seems to be associated with stable CAF. The other two, Experiments 6 and 9, are unstable to very long waves, leading to slugs whose lengths ($12.186R_2, 66.340R_2$) are nearly as long or longer than the $15.75R_2$ length of frames shown in the pictures of figure 1. We cannot distinguish such long slugs from 'oil in water concentric'. A shorter slug can be identified in Experiment 9 of figure 1 as the region between the narrow black lines running from top to bottom. The smaller water bubbles shown in Experiments 6 and 9 and the oil bubbles in Experiment 10 are unexplained by this analysis. They could arise as a reaction to turbulence in the water, or as kind of secondary instability of slugs.

14. Conclusions

The analysis of the spectral problem of linear stability leads to the following conclusions:

(1) Core–annular flow (CAF) is stable to disturbances with infinitely long wavelengths, $\alpha \to 0$ for some $\mathbb{R}_1$ when the ratio $a = R_2/R_1$ of the radius of the pipe to the mean radius of the interface does not exceed a critical value $\hat{a}(m)$ which depends on the viscosity ratio $m = \mu_2/\mu_1 \leqslant 1$ alone (see figure 4) and

$$1.4889 = \hat{a}(0.15) \leqslant \hat{a} \leqslant \hat{a}(1) = 1.5805. \tag{14.1}$$

When $a > \hat{a}$, CAF is unstable to waves $\alpha \to 0$ at any $\mathbb{R}_1$.

(2) CAF is unstable to long waves $\alpha < 1$ when the core Reynolds number $\mathbb{R} = W_0 R_1/\nu$, where W_0 is the centreline velocity, is smaller than a critical value

$$\tilde{\mathbb{R}}_{\mathrm{L}}(m, a, J^*) = \max_{\alpha \geqslant 0} \mathbb{R}_{\mathrm{cL}}(a, m, J^*, \alpha), \tag{14.2}$$

where $\mathbb{R}_{\mathrm{cL}}$ is the lower branch of the neutral curve (see figures 8–10, 13 and 14). This long-wave instability is induced by surface tension and is a generalized capillary instability which leads to the formation of oil slugs and bubbles in water. When $a > 1.5805$, this instability is always present.

(3) The limit $m \to 0, \mathbb{R}_1 > 0$ is singular and leads to inviscid flow in the water,

whereas the flow in the core reduces to the problem of capillary instability of a viscous jet which was studied by Chandrasekhar (1961). This problem depends on a surface-tension parameter $J = J^*/a = TR_1/\rho_1 \nu_1^2$. When $J \to 0$, the wavelength of the disturbance with maximum growth tends to infinity, when $J \to \infty$ then Chandrasekhar's problem reduces to Rayleigh's with a most dangerous $\alpha = 0.697$.

(4) Increasing J^* stabilizes short waves $\alpha > 1$ and destabilizes long ones $\alpha < 1$.

(5) The limit $m > 0, \mathbb{R}_1 \to 0$ is a Stokes flow limit. CAF is always unstable to long waves $\alpha < 1$ and is always stable to short waves $\alpha < 1$ in this limit when $J^* > 0$.

(6) CAF is unstable to short waves when

$$\mathbb{R}_1 > \tilde{\mathbb{R}}_U(m, a, J^*) = \min_{\alpha \geqslant 0} \mathbb{R}_{cU}(a, m, J^*, \alpha), \tag{14.3}$$

where $\mathbb{R}_{cU}$ is the upper branch associated with shorter waves, α can be greater than one (see figures 8–10 and 13–15). Instability above the upper branch appears to lead to emulsions of water in oil. The emulsions may arise as a second capillary instability after water fingers into oil.

(7) There is a window of parameters (a, m, J^*) such that CAF is stable; that is, there is an interval

$$\tilde{\mathbb{R}}_L \leqslant \mathbb{R}_1 \leqslant \tilde{\mathbb{R}}_U \tag{14.4}$$

of stable CAF. In this interval, we may say that capillary instability has been stabilized by shear. A section of such a window is shown in figure 12. This figure shows that there is an optimizing value of $m \approx 0.5$ which makes the stable interval (14.4) largest when $J^* = 930$ and $a = 1.25$.

(8) The density difference, without gravity, affects the stability of CAF, with opposite effects on the lower and upper branches. If we increase $\zeta_2 = \rho_2/\rho_1$ so that the fluid in the annulus is more dense, then $\mathbb{R}_{cL}$ is decreased and there is a smaller region of generalized capillary instability; that is, the lower branch is more stable. The effect on the upper branch is opposite; increasing ζ_2, decreases $\mathbb{R}_{cU}$ increasing the region $\mathbb{R}_1 > \mathbb{R}_{cU}$ of instability. The destabilizing effect of increasing ζ_2 on the upper branch is much greater than the stabilizing effect on the lower branch (see figure 11.2).

(9) The numerical results show that there is a critical Reynolds number in the water

$$Re = \tilde{\mathbb{R}}_U(a-1)/m.$$

Hence,

$$\tilde{\mathbb{R}}_U = \frac{m}{a-1} Re.$$

In the experiment, $Re \approx 660$ is nearly independent of a for $a \leqslant 1.42$. Hence,

$$\tilde{\mathbb{R}}_U \approx \frac{35.2}{a-1}.$$

On the other hand, $\tilde{\mathbb{R}}_L$ increases monotonically from zero when $a = 1$ to ∞ at a finite a (cf. figure 6). It follows that the interval (13.4) of stable CAF is maximal $0 < \mathbb{R}_1 < \infty$, when $a \to 1$.

(10) There is a critical value $a = \tilde{a}(m, J^*)$ such that when $a > \tilde{a}$, the interval (14.4) of stable CAF closes (see figure 9) and CAF is unstable. Moreover,

$$\tilde{a}(m, J^*) \leqslant \hat{a}(m).$$

For $m = 0.0532, J^* = 2102$, corresponding to experiments of CGH (1961),

$$\tilde{a} \approx 1.23$$

(see figure 17). It is arguable that one of the most important parameters in lubricated pipelining is the volume fraction of oil to water

$$\phi = \frac{V_W}{V_O} = \frac{\pi(R_2^2 - R_1^2)}{\pi R_1^2} = a^2 - 1.$$

In the experiments, CAF is unstable when $\phi > 0.5376$. The pictures of the experiments shown in figure 1 suggest that long slugs are stable in a lubricated flow with $a \approx 1.2$.

(11) The linear theory of stability has shown that all the cases of emulsified water drops in oil seen in the experiments of CGH (1961), and only these cases, are at Reynolds number exciting the short waves on the upper branch $\mathbb{R}_1 > \tilde{\mathbb{R}}_U$ and that long waves are not excited $\mathbb{R}_1 > \tilde{\mathbb{R}}_L$ (see figures 13 and 14).

This work was supported by the Department of Energy; the National Science Foundation, Fluid Mechanics and the Army Research Office, Mathematics. Computer results were obtained under a grant from the Academic Computing Services and Systems of the University of Minnesota.

REFERENCES

CHANDRASEKHAR, S. 1961 *Hydrodynamics and Hydromagnetic Stability*. Dover.

CHARLES, M. E., GOVIER, G. W. & HODGSON, G. W. 1961 The horizontal pipeline flow of equal density of oil–water mixtures. *Can. J. Chem. Engng* **39**, 17–36.

CHARLES, M. E. & LILLELEHT, L. U. 1966 Correlation of pressure gradients for the stratified laminar-turbulent pipeline flow of two immiscible liquids. *Can. J. Chem. Engng* **44**, 47–49.

GEMMEL, A. R. & EPSTEIN, N. 1962 Numerical analysis of stratified laminar flow of two immiscible Newtonian liquids in circular pipes. *Can. J. Chem. Engng* **40**, 215–224.

HESLA, T. I., PRANCKH, F. R. & PREZIOSI, L. 1986 Squire's theorem for two stratified fluids. *Phys. Fluids* **29**, 2808–2811.

HICKOX, C. E. 1971 Instability due to viscosity and density stratification in axisymmetric pipe flow. *Phys. Fluids* **14**, 251–262.

HOOPER, A. & BOYD, W. G. 1983 Shear-flow instability at the interface between two viscous fluids. *J. Fluid Mech.* **128**, 507–528.

HOOPER, A. & BOYD, W. G. 1987 Shear flow instability due to a wall and a viscosity discontinuity at the interface. *J. Fluid Mech.* **179**, 201–225.

JOSEPH, D. D. 1976 *Stability of Fluid Motions*. Springer.

JOSEPH, D. D., NGUYEN, K. & BEAVERS, G. S. 1984 Non-uniqueness and stability of the configuration of flow of immiscible fluids with different viscosities. *J. Fluid Mech.* **141**, 319–345.

JOSEPH, D. D., RENARDY, M. & RENARDY, Y. 1983 Instability of the flow of immiscible liquids with different viscosities in a pipe. *Math. Res. Center Tech. Summary Rep.* 2503.

JOSEPH, D. D., RENARDY, Y. & RENARDY, M. 1984 Instability of the flow of immiscible liquids with different viscosities in a pipe. *J. Fluid Mech.* **141**, 309–317.

OLIEMANS, R. V. A. 1986 *The Lubricating Film Model for Core-annular Flow*. Delft University Press.

OLIEMANS, R. V. A. & OOMS, G. 1986 Core–annular flow of oil and water through a pipeline. In *Multiphase Science & Technology*, Vol. 2 (ed. G. F. Hewitt, J. M. Delhaye & N. Zuber). Hemisphere.

ORSZAG, S. A. & KELLS, L. C. 1980 Transition to turbulence in plane Poiseuille and plane Couette flow. *J. Fluid Mech.* **96**, 159–205.

RAYLEIGH, LORD 1879 On the instability of jets. *Proc. Lond. Math. Soc.* **10**, 4–13.

RENARDY, M. & JOSEPH, D. D. 1986 Hopf bifurcation in two-component flow. *SIAM J. Math. Anal.* **17**, 894–910.

RENARDY, Y. 1985 Instability at the interface between two shearing fluids in a channel. *Phys. Fluids* **28**, 3411–3443.

RENARDY, Y. & JOSEPH, D. D. 1985 Couette flow of two fluids between concentric cylinders. *J. Fluid Mech.* **150**, 381–394.

RUSSELL, T. W. F. & CHARLES, M. E. 1959 The effect of the less viscous liquid in the laminar flow of two immiscible liquids. *Can. J. Chem. Engng* **39**, 18–24.

RUSSELL, T. W. F., HODGSON, G. W. & GOVIER, G. W. 1959 Horizontal pipeline flow of mixtures of oil and water. *Can. J. Chem. Engng* **37**, 9–17.

SALWEN, H., COTTON, F. W. & GROSCH, C. E. 1980 Linear stability of Poiseuille flow in a circular pipe. *J. Fluid Mech.* **98**, 273–284.

SALWEN, H. & GROSCH, C. E. 1972 The stability of Poiseuille flow in a pipe of circular cross-section. *J. Fluid Mech.* **54**, 93–112.

THAN, P., ROSSO, F. & JOSEPH, D. D. 1987 Instability of Poiseuille flow of two immiscible liquids with different viscosities in a channel. *Intl J. Engng Sci.* **25**, 189.

YIH, C. S. 1967 Instability due to viscosity stratification. *J. Fluid Mech.* **27**, 337.